



HAL
open science

Adenomatous Polyposis Coli Defines Treg Differentiation and Anti-inflammatory Function through Microtubule-Mediated NFAT Localization

Sonia Agüera-Gonzalez, Oliver T. Burton, Elena Vázquez-Chávez, Céline Cucho, Floriane Herit, Jérôme Bouchet, Rémi Lasserre, Iratxe del Río-Iñiguez, Vincenzo Di Bartolo, Andres Alcover

► To cite this version:

Sonia Agüera-Gonzalez, Oliver T. Burton, Elena Vázquez-Chávez, Céline Cucho, Floriane Herit, et al.. Adenomatous Polyposis Coli Defines Treg Differentiation and Anti-inflammatory Function through Microtubule-Mediated NFAT Localization. *Cell Reports*, 2017, 21 (1), pp.181-194. 10.1016/j.celrep.2017.09.020 . hal-01614654

HAL Id: hal-01614654

<https://hal.science/hal-01614654>

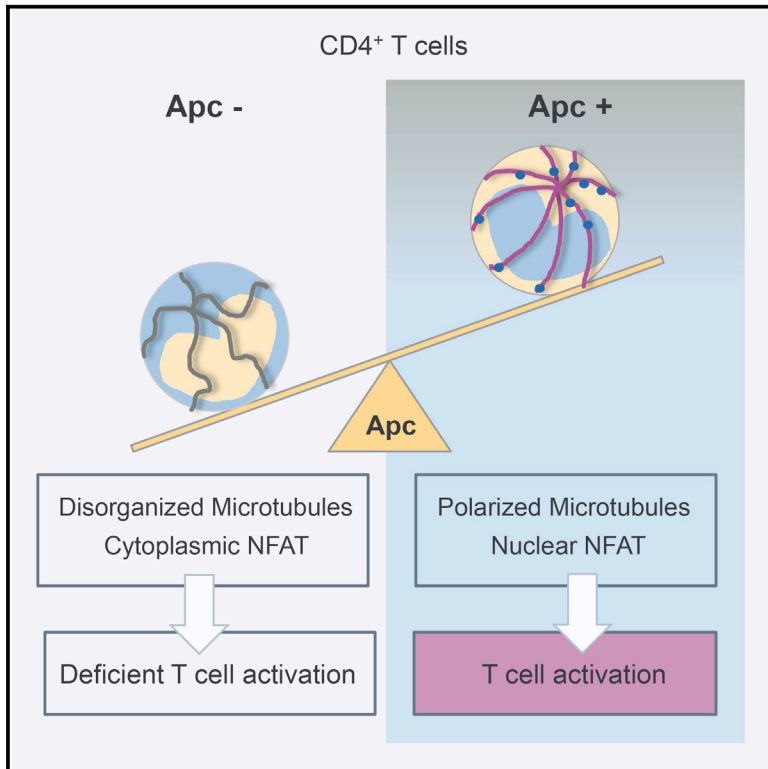
Submitted on 11 Oct 2017

HAL is a multi-disciplinary open access archive for the deposit and dissemination of scientific research documents, whether they are published or not. The documents may come from teaching and research institutions in France or abroad, or from public or private research centers.

L'archive ouverte pluridisciplinaire **HAL**, est destinée au dépôt et à la diffusion de documents scientifiques de niveau recherche, publiés ou non, émanant des établissements d'enseignement et de recherche français ou étrangers, des laboratoires publics ou privés.

Adenomatous Polyposis Coli Defines Treg Differentiation and Anti-inflammatory Function through Microtubule-Mediated NFAT Localization

Graphical Abstract



Authors

Sonia Agüera-González, Oliver T. Burton, Elena Vázquez-Chávez, ..., Iratxe del Río-Iñiguez, Vincenzo Di Bartolo, Andrés Alcover

Correspondence

sonia.aguera-gonzales@curie.fr (S.A.-G.), andres.alcover@pasteur.fr (A.A.)

In Brief

Agüera-González et al. investigate the role of the polarity regulator and tumor suppressor *Adenomatous polyposis coli* (APC) in CD4 T cell activation and effector function. APC controls microtubule reorganization, NFAT transcription factor localization, and cytokine gene expression. In *Apc*^{Min/+} mutant mice, regulatory T cell (Treg) differentiation and anti-inflammatory function were intrinsically affected.

Highlights

- APC controls microtubule organization and NFAT-driven cytokine gene expression
- APC silencing impairs NFAT nuclear localization and activation
- NFAT associates with microtubules that control its localization and its activation
- *Apc*^{Min/+} Tregs have intrinsically reduced differentiation and IL-10 production



Adenomatous Polyposis Coli Defines Treg Differentiation and Anti-inflammatory Function through Microtubule-Mediated NFAT Localization

Sonia Agüera-González,^{1,2,3,5,9,*} Oliver T. Burton,^{4,8} Elena Vázquez-Chávez,^{1,2,3} Céline Cuhe,^{1,2,3} Floriane Herit,^{1,2,3,6} Jérôme Bouchet,^{1,2,3,6} Rémi Lasserre,^{1,2,3,7} Iratxe del Río-Iñiguez,^{1,2,3} Vincenzo Di Bartolo,^{1,2,3} and Andrés Alcover^{1,2,3,*}

¹Institut Pasteur, Department of Immunology, Lymphocyte Cell Biology Unit

²CNRS URA1961

³INSERM U1221

75015 Paris, France

⁴Division of Immunology, Boston Children's Hospital and Department of Pediatrics, Harvard Medical School, Boston, MA 02115, USA

⁵Present addresses: Institut Curie, Membrane and Cytoskeleton Dynamics Group, CNRS UMR144, 75005 Paris, France

⁶Present addresses: Institut Cochin, INSERM, U1016, CNRS, UMR8104, Université Paris Descartes, Sorbonne Paris Cité, 75014 Paris, France

⁷Present addresses: Centre d'Immunologie de Marseille-Luminy, Aix Marseille Université UM2, Inserm, U1104, CNRS UMR7280, 13288 Marseille, France

⁸Present addresses: Department of Microbiology and Immunology, VIB, University of Leuven, 3000 Leuven, Belgium

⁹Lead Contact

*Correspondence: sonia.aguera-gonzales@curie.fr (S.A.-G.), andres.alcover@pasteur.fr (A.A.)

<http://dx.doi.org/10.1016/j.celrep.2017.09.020>

SUMMARY

Adenomatous polyposis coli (APC) is a polarity regulator and tumor suppressor associated with familial adenomatous polyposis and colorectal cancer development. Although extensively studied in epithelial transformation, the effect of APC on T lymphocyte activation remains poorly defined. We found that APC ensures T cell receptor-triggered activation through Nuclear Factor of Activated T cells (NFAT), since APC is necessary for NFAT's nuclear localization in a microtubule-dependent fashion and for NFAT-driven transcription leading to cytokine gene expression. Interestingly, NFAT forms clusters juxtaposed with microtubules. Ultimately, mouse *Apc* deficiency reduces the presence of NFAT in the nucleus of intestinal regulatory T cells (Tregs) and impairs Treg differentiation and the acquisition of a suppressive phenotype, which is characterized by the production of the anti-inflammatory cytokine IL-10. These findings suggest a dual role for APC mutations in colorectal cancer development, where mutations drive the initiation of epithelial neoplasms and also reduce Treg-mediated suppression of the detrimental inflammation that enhances cancer growth.

INTRODUCTION

T lymphocytes recognize peptide antigens associated with major histocompatibility complex molecules (MHCs) on antigen-presenting cells. Antigen recognition induces T cell polarization

toward the antigen-presenting cell. This forms an organized interface, the immunological synapse that regulates T cell activation leading to T cell growth, differentiation and cytokine production. T cell receptor (TCR) and signaling molecules dynamically concentrate at the immunological synapse to optimally control T cell activation. This depends on the orchestrated action of the actin and microtubule cytoskeleton, and intracellular vesicle traffic (Agüera-Gonzalez et al., 2015; Soares et al., 2013).

Cell polarity is regulated by an array of evolutionary conserved polarity complexes crucial for stably polarized epithelial cells (Rodríguez-Boulan and Macara, 2014) or for induced polarization in migrating cells (Elric and Etienne-Manneville, 2014). Scribble, Dlg1, and PKC ζ polarity regulators were shown to control lymphocyte migration, immunological synapse formation, and T cell activation (Bertrand et al., 2010; Lasserre et al., 2010; Ludford-Menting et al., 2005; Real et al., 2007; Round et al., 2007; Xavier et al., 2004).

The polarity regulator and tumor suppressor adenomatous polyposis coli (APC) is known for its association with familial adenomatous polyposis (FAP), large numbers of sporadic human colorectal tumors, and intestinal carcinomas in mice (McCartney and Näthke, 2008; Moser et al., 1990; Su et al., 1992; Zeineldin and Neufeld, 2013). APC contains several protein-protein interaction domains (Figure 1A), permitting its involvement in various cellular processes including proliferation, differentiation, migration, and death. APC-interacting proteins include β -catenin, the polarity regulators Dlg1 or Scribble, cytoskeleton regulators, nuclear pore and nuclear transport proteins, and apoptosis- or mitosis-related proteins (Etienne-Manneville, 2009; Nelson and Näthke, 2013).

The effect of APC mutations on intestinal epithelium differentiation and tumor progression has been widely investigated in colorectal cancer patients and in mouse models (Bérout and Soussi, 1996; McCartney and Näthke, 2008; Moser et al.,

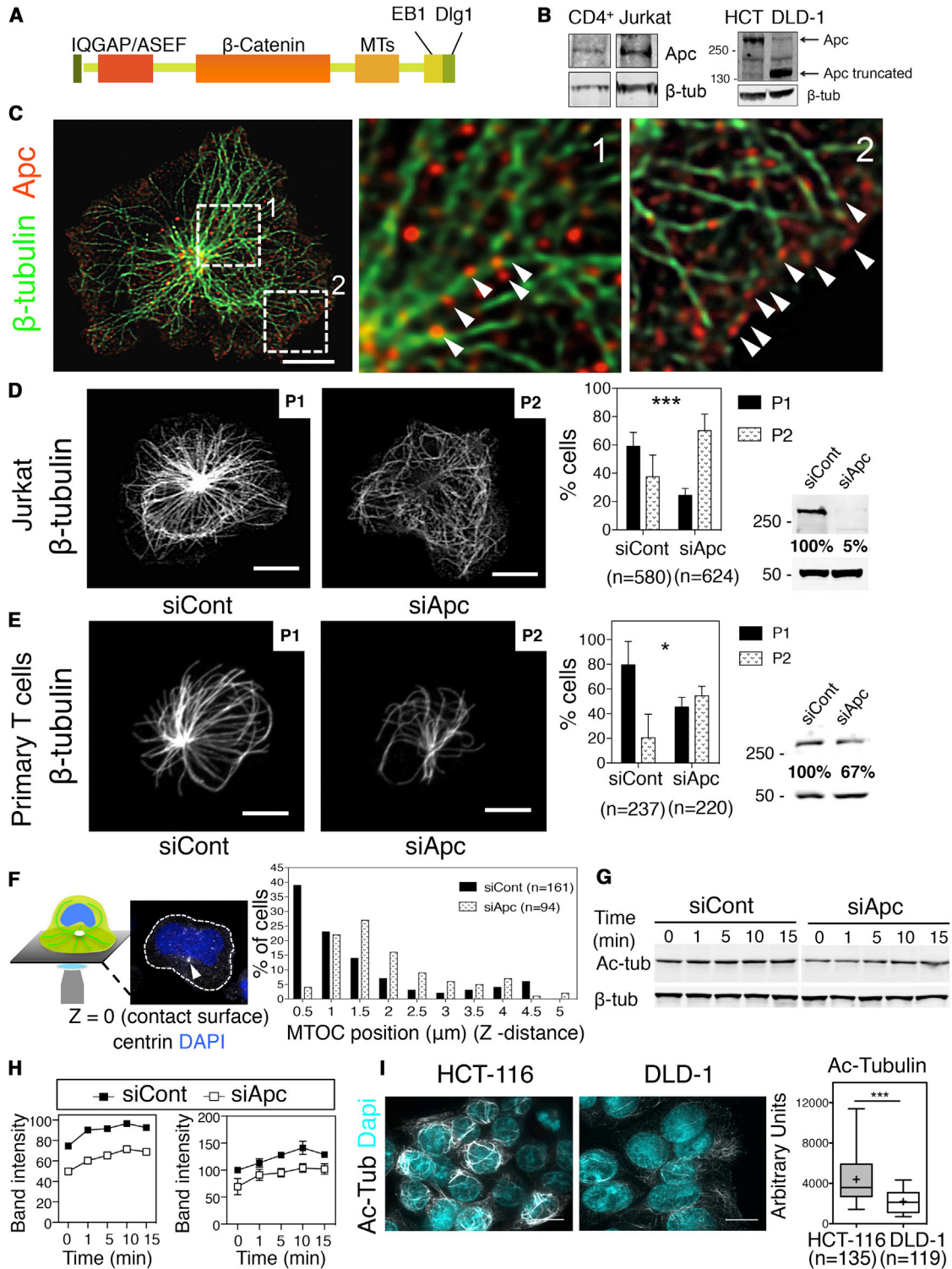


Figure 1. APC Is Expressed in T Cells and Controls Microtubule Network Organization upon TCR Stimulation

(A) Scheme of APC protein interaction motifs.

(B) Expression of APC in primary human CD4⁺ T cells (CD4⁺), Jurkat T cells, and colorectal carcinoma cell lines (HCT-116, DLD-1).

(C) Immunofluorescence of APC (red, arrowheads) and microtubules (green) at the immunological pseudo synapses (anti-CD3-coated coverslips 3 min). Scale bar, 3 μm.

(legend continued on next page)

1990; Nelson and Näthke, 2013; Su et al., 1992; Zeineldin and Neufeld, 2013). Altered intestinal immune homeostasis was found in *Apc* mutant mice, together with the impaired control of inflammation by regulatory T lymphocytes (Tregs) (Akeus et al., 2014; Chae and Bothwell, 2015; Gounaris et al., 2009). However, whether *Apc* defects in T cells contribute to this loss of anti-inflammatory functions remains only vaguely explored (Tanner et al., 2016). Our data unveil the requirement for APC in T cell receptor-dependent nuclear factor of activated T cells (NFAT) activation. APC permits NFAT nuclear localization in a microtubule-dependent fashion. Moreover, *Apc*^{Min/+} mice display modestly reduced levels of NFAT expression and nuclear localization in intestinal regulatory T cells (Tregs). Heteroinsufficiency of *Apc* leads to induced Treg (iTreg) populations with impaired capacity to differentiate and produce NFAT-regulated cytokines, particularly interleukin-10 (IL-10), which is essential to control intestinal inflammation and adenocarcinoma progression (Rubtsov et al., 2008).

RESULTS

APC Regulates Microtubule Network Organization at the Immunological Synapse

We first investigated the expression of APC in human T cells. Jurkat cells and peripheral blood T cells express apparent full-length APC (311 kDa), as compared with HCT-116 and DLD-1 colon cancer cell lines that express full-length and truncated APC forms, respectively (Bérout and Soussi, 1996) (Figure 1B). We then localized APC in T cells. As we have previously shown (Lasserre et al., 2010), T cells on stimulatory anti-CD3-coated coverslips (pseudo synapses) display radially organized microtubules, with the centrosome apposed to the contact site (Figures 1C–1E). Similar to other cell types (Etienne-Manneville et al., 2005; Näthke et al., 1996), APC appeared as discrete puncta apposed to microtubules (Figure 1C; Movie S1), frequently localized at the synapse periphery, likely corresponding to microtubule tips, as shown at the leading edge of migrating cells (Etienne-Manneville et al., 2005) (Figure 1C, right, arrowheads; Movie S1).

APC regulates microtubule stability and organization in polarized cells (Etienne-Manneville et al., 2005; Kroboth et al., 2007; Mogensen et al., 2002). We therefore investigated the role of APC in microtubule network organization at the immunological synapse. We assessed microtubule patterns at pseudo synapses of control and APC-silenced T cells. Control T cells mostly displayed radial microtubule patterns, whereas APC-silenced cells frequently displayed disorganized microtubule patterns in both Jurkat and primary T cells (Figures 1D and 1E). Moreover,

centrosome polarization to the immunological synapse was less efficient in APC-silenced cells, as assessed by the centrosome distance to the contact site (Figure 1F).

Tubulin acetylation correlates with microtubule stability and is controlled by APC (Kroboth et al., 2007). Consistently, APC-silenced T cells had lower levels of acetylated tubulin in unstimulated and CD3+CD28-stimulated cells (Figures 1G and 1H). Lower tubulin acetylation was also observed in DLD-1 epithelial carcinoma cells expressing truncated APC (Figure 1I) and in CD4⁺ and Tregs from *Apc*^{Min/+} heterozygous mutant mice (Figures S2B and S2H).

In sum, APC depletion results in impaired microtubule acetylation, microtubule network organization, and centrosome polarization at the immunological synapse.

APC Silencing Alters Microcluster Patterns without Affecting Early TCR Signaling

Immunological synapses direct T cell activation through the actin- and microtubule-dependent spatial and temporal organization of TCR signaling complexes (Bunnell et al., 2002; Campi et al., 2005; Lasserre et al., 2010; Yokosuka et al., 2005). APC silencing affected the generation and dynamics of signaling complexes at the immunological synapse, as monitored by the number, intensity, and trajectories of YFP-SLP76 microclusters (Figures S1A and S1B, arrowheads, and S1C and S1D). However, APC-silenced cells did not have altered tyrosine phosphorylation of the proximal TCR signaling molecules ZAP70 and PLC γ 1, or calcium flux (Figures S1E–S1H; Movies S6 and S7).

Therefore, APC is necessary for the generation and dynamics of signaling microcluster at the immunological synapse, without significantly affecting early signaling.

APC Regulates NFAT-Driven Gene Transcription

The transcription factors NFAT, nuclear factor κ B (NF- κ B), and AP1 (Fos and Jun) are crucial for antigen-triggered T cell growth, differentiation, and cytokine gene regulation. We investigated the effect of APC silencing on NFAT-, NF- κ B-, and AP1-driven transcription using luciferase expression vectors. Despite normal TCR-induced phosphorylation and Ca²⁺ flux in APC-silenced cells (Figures S1E–S1H), NFAT-driven luciferase expression was significantly lower (Figure 2A). In contrast, NF- κ B- or AP1-driven luciferase was not affected (Figure 2B and 2C). Similar effects were observed when T cells were stimulated with calcium ionophore (Iono) and phorbol myristate acetate (PMA) that activate calcineurin and protein kinase C (PKC), respectively, bypassing TCR proximal signal events (Figures 2D–2F). Moreover, APC silencing decreased *IL2* gene expression in Jurkat and primary T cells, as assessed by qRT-PCR (Figures 2G and 2H).

(D and E) Microtubule network organization in siRNA control (siCont) or APC (siAPC) in Jurkat (D) and primary human CD4⁺ T lymphocytes (E). Cells were ranked in two categories: pattern 1 (P1), presence of a radial plane of microtubules, or pattern 2 (P2), non-radial organization. APC expression was measured by western blot. Data are representative of three experiments (Jurkat) and two experiments for primary T cells (mean \pm SD, two-way ANOVA). Scale bar, 3 μ m.

(F) Centrosome position in siCont and siAPC Jurkat cells (distance of centrin spot to the coverslip). Data are representative of two experiments.

(G and H) Tubulin acetylation (Ac-Tub) in siCont and siAPC Jurkat cells activated with soluble anti-CD3+CD28 antibodies (Abs). Ac-Tub band was normalized to control β -tubulin and the percentage of siCont at time 0. Data are representative of three experiments (blot, G, and left graph, H). Mean \pm SD of three experiments (H, right graph).

(I) Ac-Tub staining in HCT-116 and DLD-1 cells. Data are from three experiments (whiskers: 5th–95th percentile; mean \pm SD; Mann-Whitney test).

See also Figure S1.

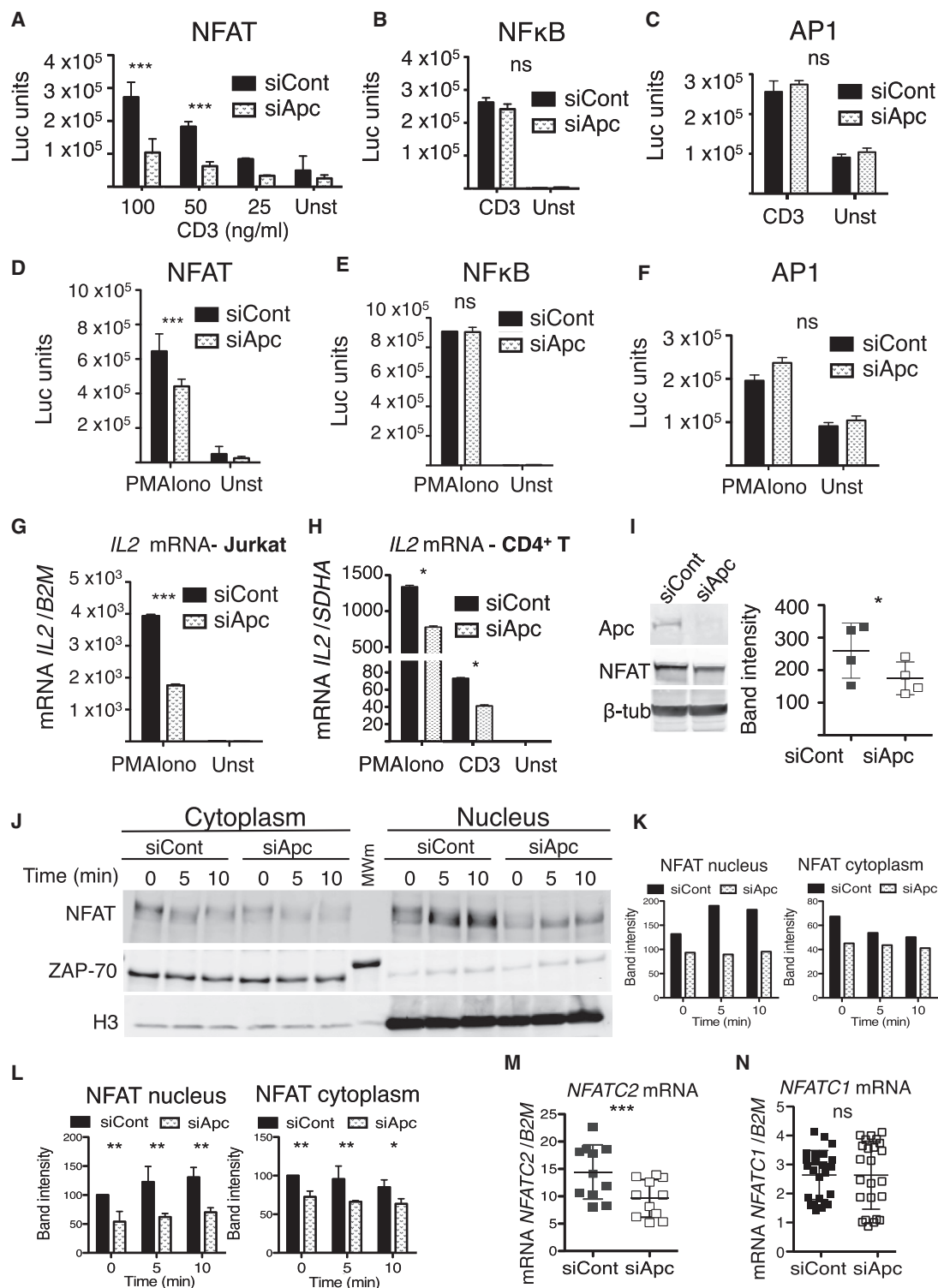


Figure 2. Effect of APC Silencing on NFAT Activation and IL2 Gene Transcription

(A–F) NFAT (A and D), NF-κB (B and E), and AP-1 (C and F)-dependent activation in siCont and siAPC Jurkat cells was measured using luciferase expression vectors. Cells were stimulated with anti-CD3+CD28 Abs (A–C) or PMA-Iono (D–F). Data are representative of six experiments for NFAT and AP1 (A, C, D, and F) and three experiments for NF-κB (B and E) (mean ± SEM, two-way ANOVA).

(G–H) IL2 mRNA quantified by qRT-PCR in siAPC Jurkat (G) and primary human T cells (H) stimulated with PMA-Iono or CD3+CD28. Data are representative six experiments in (G) and of three experiments in (H) (mean ± SD; Mann-Whitney test).

(legend continued on next page)

Similarly, T cells from mice with heteroinsufficiency for Apc ($Apc^{Min/+}$) exhibited reduced proliferative, cytokine production and Treg lineage commitment responses to TCR stimulation compared to their wild-type counterparts (Figures S2A and S2C–S2G). Moreover, the early response gene *c-Myc* was also inhibited (Figures S2B and S2H).

NFAT shuttles between the cytoplasm and the nucleus in a phosphorylation-dependent manner. Cytoplasmic NFAT is phosphorylated on several serine residues whose dephosphorylation by the calcium-dependent phosphatase calcineurin drives NFAT nuclear translocation and gene transcription (Beals et al., 1997a; Okamura et al., 2000). Conversely, phosphorylation by the serine kinases GSK-3 β facilitates NFAT nuclear export and cytoplasmic retention (Beals et al., 1997b; Shibasaki et al., 1996).

We investigated the effect of APC silencing on NFATC2 (NFAT1), an isoform constitutively expressed in T cells, which concentrates in the nucleus in response to TCR-CD28 stimulation or PMA-Iono. Nuclear NFATC2 in APC-silenced activated Jurkat or primary T cells was lower compared to controls. (Figures 2J–2L, S3A, and S3B). Similarly, DLD-1 carcinoma cells expressing truncated APC were less efficient at translocating NFATC2 and producing NFAT-driven luciferase in response to PMA-Iono than HCT-116 controls (Figures S3C and S3D). Moreover, we observed that NFATC2 was less expressed at the mRNA and protein level in APC-silenced Jurkat cells (Figures 2I and 2M), whereas NFATC1 (NFAT2) isoform expression was not significantly affected (Figure 2N).

Since APC and GSK-3 form a complex (Stamos and Weis, 2013), and GSK-3 phosphorylates NFAT and regulates its nuclear-to-cytoplasmic cycling (Beals et al., 1997b), we investigated whether APC silencing affects NFATC2 phosphorylation. We therefore analyzed NFATC2 phosphorylation status by comparing its electrophoretic mobility. Bands with slower mobility represent more phosphorylated protein species. Apc silencing did not significantly affect the ratio of higher to lower mobility NFAT electrophoretic bands, suggesting that phosphorylation was not altered by APC depletion (Figures S4A–S4H).

In sum, APC is necessary for NFATC2 expression and nuclear localization, as well as NFAT-driven gene transcription with functional consequences for proliferation, differentiation, and cytokine expression.

NFAT Nuclear Localization and Activation Requires Microtubule Integrity

Microtubule disorganization in APC-silenced cells (Figures 1D–1F) prompted us to hypothesize that APC regulation of microtubules may influence NFAT activation, including nuclear localization and transcriptional activity. Therefore, we first analyzed NFATC2 localization with respect to microtubules. We observed discrete puncta of endogenous NFATC2 juxtaposed to microtubules (Figure 3A, arrowheads). We then measured the distance

of NFATC2 microclusters to the closest microtubule at different activation times, using 3D segmentations and quantitative image analysis (Figures 3B and 3C; Movies S2, S3, S4, and S5). NFATC2-microtubule distance was $\approx 0.2 \mu\text{m}$ in non-stimulated cells and significantly increased upon TCR stimulation (Figures 3C and 3D). NFATC2 microclusters approached to the synapse surface at early activation times and then progressively moved away to a central, peri-nuclear region of the cell as the cell retracted from the coverslip (Z-position; Figure 3E). The number of NFAT microclusters was conserved during the course of T cell activation (Figure 3F). These data are consistent with NFATC2 forming microclusters associated with microtubules in resting and early activated T cells and then separating at later times as NFAT translocates to the nucleus.

It was reported that NFAT and APC form cytoplasmic complexes that share common partners, like the Ser/Thr kinase GSK-3 β , and the cytoskeleton regulator IQGAP (Sharma et al., 2011; Stamos and Weis, 2013). Moreover, both APC and NFAT associate with microtubules displaying spotted patterns (Figures 1C and 3A). Therefore, we investigated the relative localization of APC and NFAT. APC and NFAT microclusters did not fully overlap, although they were often found in close proximity (Figure 3G, arrowheads).

Next, we investigated whether microtubule integrity was required for NFATC2 localization and transcriptional activity. Treatment of T cells with the microtubule polymerization inhibitor colchicine significantly reduced the number of NFAT clusters at the immunological synapse, providing further evidence of the close relationship between NFAT and the microtubule network (Figure 4A). Furthermore, colchicine significantly inhibited NFAT-driven luciferase gene expression under both CD3-CD28 and PMA-Iono T cell stimulations (Figures 4B and 4C). Consistently, IL2 mRNA levels were reduced in colchicine-treated cells (Figure 4D). In addition, NFAT nuclear detection was significantly reduced in colchicine-treated T cells (Figures 4E–4G), suggesting that the defect of NFAT-dependent transcription could be related to impaired NFAT nuclear localization. In contrast with APC-silenced cells, colchicine-treated T cells displayed comparable amounts of total NFAT protein and mRNA (Figures 4H and 4I), suggesting that NFAT nuclear localization could be microtubule-dependent.

Finally, overexpression of two APC truncated molecules containing the C-terminal APC microtubule and EB1 interacting regions (Etienne-Manneville et al., 2005) significantly inhibited NFAT-driven luciferase expression in Jurkat cells, although less efficiently than APC silencing (Figure 4J).

Altogether, our data indicate that APC controls NFAT-driven gene transcription by regulating NFAT nuclear localization in a microtubule-dependent manner. APC also affects NFAT mRNA and protein levels. APC silencing inhibits NFAT, without altering NF- κ B or AP1, leading to reduced IL2 gene expression.

(I) NFAT expression by western blot in APC-silenced cells. Data are representative of four experiments (two-tailed paired t test).

(J–L) Nuclear NFATC2 detection by western blot of cytoplasmic-nuclear fractionations (J) (ZAP-70 cytoplasmic control and histone-3 nuclear). Data are representative of three experiments (K). Mean \pm SD of three experiments (L), two-way ANOVA.

(M and N) NFATC2 (M) and NFATC1 (N) mRNA quantification by qRT-PCR. Data are representative of four experiments (M) and eight experiments (N) (mean \pm SD; Mann-Whitney test).

See also Figure S2.

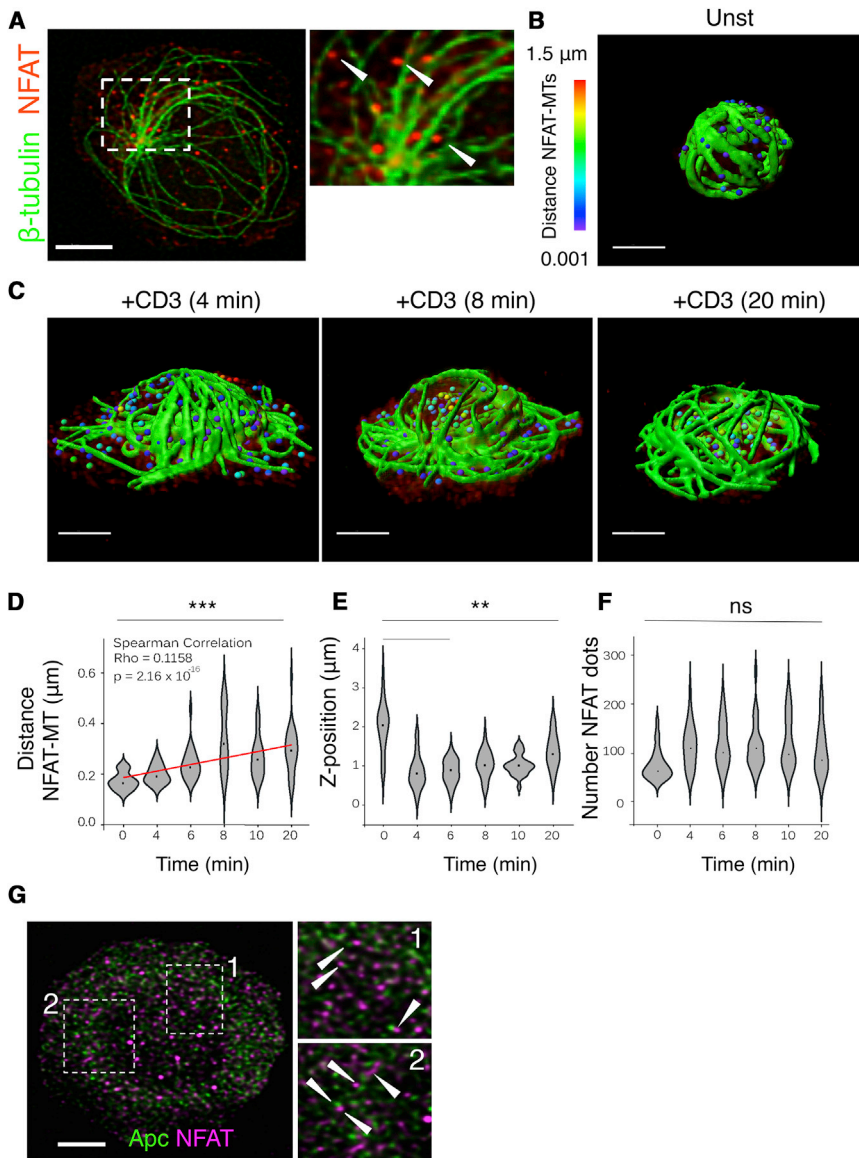


Figure 3. NFATC2 and Microtubule Localization

(A–F) Endogenous NFATC2 (red) and microtubules (green) in human primary CD4⁺ T cells activated on anti-CD3-coated coverslips.

(A) Cell-coverslip contact site. Arrowheads indicate NFAT clusters. Scale bar, 3 μ m.

(B and C) 3D visualization of NFAT (distance-dependent colored dots) and microtubules (green) in unstimulated (B) or 4–8–20 min stimulated (C) cells.

(D) NFAT-microtubule mean distance per cell (Spearman correlation = 0.11).

(E) Distance of NFAT to coverslip (mean per cell). (F) Number of NFAT dots per cell. Data are representative of three experiments (Kruskal-Wallis test of one-way ANOVA).

(G) NFATC2 (green) and APC (magenta) detection in human primary CD4⁺ T cells on anti-CD3-coated coverslips. Data are representative of three experiments. Scale bar, 3 μ m. See also Figure S3.

but significant change in the cellular distribution of NFAT in mutant Tregs, with a shift away from the nucleus (Figure 5A). Moreover, conventional flow cytometric analysis confirmed a significant reduction in Foxp3 protein levels within *Apc*^{Min/+} Treg (Figure 5B). Further investigation into Treg phenotypes revealed a dramatic shift in Treg subtypes populating the intestine of *Apc*^{Min/+} mice, with a marked reduction in frequencies of ROR γ t⁺ Tregs that are induced in response to environmental cues and are required for the control of inflammation at mucosal surfaces (Ohnmacht et al., 2015; Yang et al., 2016) (Figure 5C). There was a counterbalancing increase in the frequency of thymus-derived, Helios^{bright} Treg (Figure 5D). These findings suggest that the ability to either generate or stably maintain this induced ROR γ t⁺ Treg population is impaired without full *Apc* function.

ROR γ t⁺ Tregs display potent suppressive activity against intestinal inflammation, and have been noted to produce IL-10, which is critical to this process (Lochner et al., 2008; Ohnmacht et al., 2015; Rubtsov et al., 2008; Yang et al., 2016). Loss of Treg suppressive function has been shown to contribute to inflammatory pathology and the growth of intestinal neoplasms in *Apc*^{Min/+} mice, and deficient IL-10 production has been implicated (Chae and Bothwell, 2015; Chung et al., 2014; Dennis et al., 2015; Kim et al., 2006; Serebrennikova et al., 2012). We therefore examined the impact of *Apc* on Treg production of IL-10, assessing cytokine production by flow cytometry. We observed a dramatic reduction in IL-10 production by Tregs in the intestine of *Apc*^{Min/+} (Figure 5E). Because Tregs are the main source of IL-10-producing T cells in the intestinal lamina propria, this loss of

Apc Controls Cytokine Gene Expression by Lamina Propria Tregs

Unlike conventional T cells, Tregs constitutively retain some NFAT in the nucleus, even in the absence of TCR stimulation (Li et al., 2012; Vaeth et al., 2012). This nuclear NFAT fraction is required to maintain a suppressive phenotype, as it cooperates with Foxp3 to drive the Treg transcriptional profile and enhances Foxp3 expression (Tone et al., 2008; van der Veen et al., 2013; Wu et al., 2006). Because we showed that APC was necessary for optimal accumulation of NFAT in the nucleus of human T cells activated in vitro, we examined the impact of *Apc* mutation on NFAT localization in Tregs isolated from the intestinal lamina propria of pre-cancerous (11-week-old) *Apc*^{Min/+} mice. Using high-throughput image analysis with imaging flow cytometry, we assessed the nuclear localization of NFAT in Tregs from wild-type (WT) and *Apc*^{Min/+} mice, finding a small

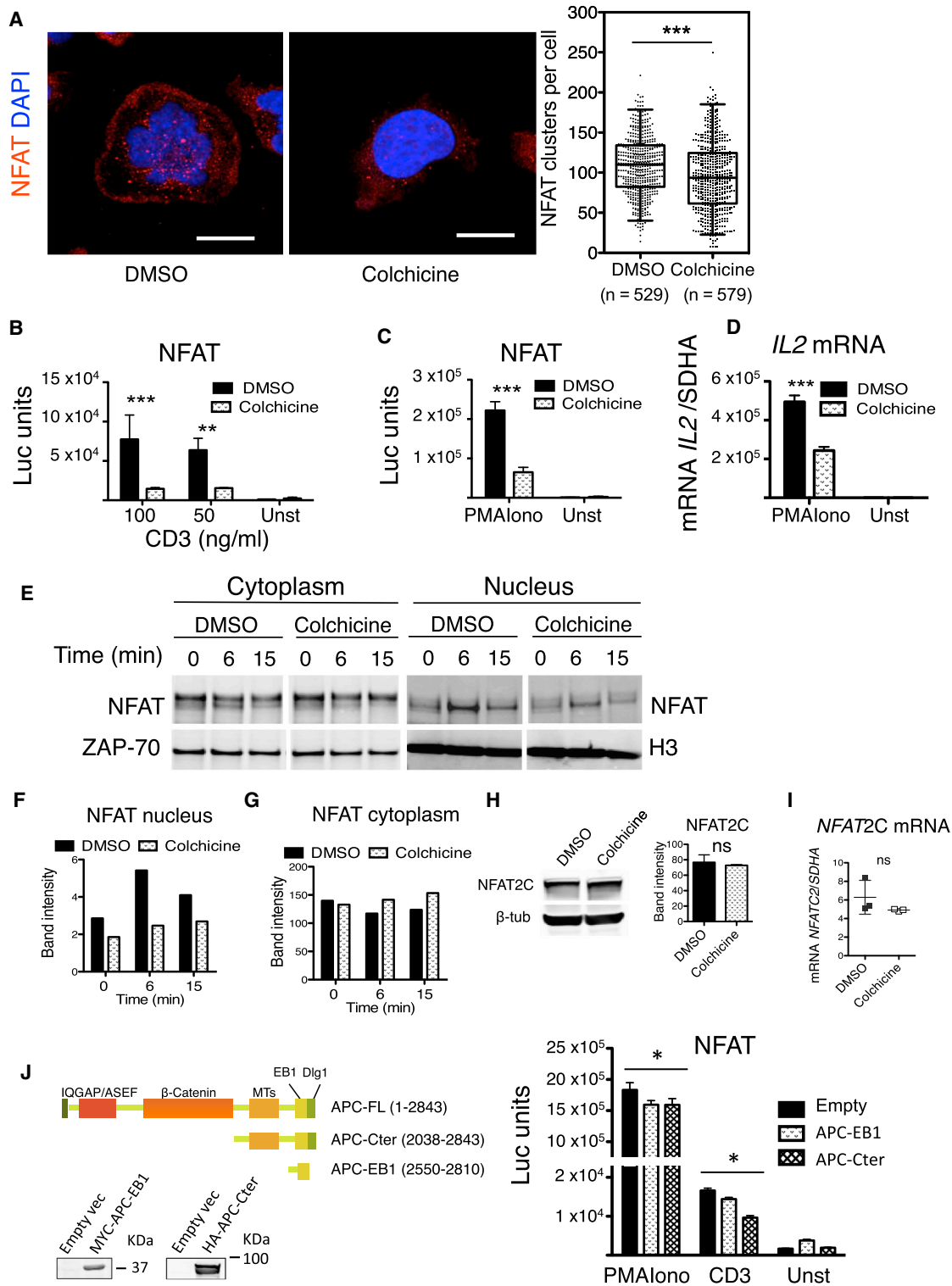


Figure 4. NFAT-Dependent T Cell Activation under Microtubule Disruption

(A) Number of NFATC2 clusters in Jurkat cells (DMSO or colchicine) on anti-CD3-coated coverslips and observed by confocal microscopy. Scale bar, 3 μ m. Data are representative of two experiments (whiskers: 2.5th–97.5th percentile; mean \pm SD; Mann-Whitney test).

(B and C) NFAT-driven luciferase expression in Jurkat cells (DMSO or colchicine), stimulated with anti-CD3+CD28 Abs (B) or PMA-Iono (C). Data are representative of four experiments (mean \pm SD; two-way ANOVA).

(legend continued on next page)

IL-10 was also observed at the level of the entire CD4⁺ T cell population (Figure S5B). We also observed a reduction in total CD4⁺ T cell production of IL-2 and IFN γ (Figures S5C and S5E), but did not observe alterations in IL-17 expression at this early time point (11-week-old mice) (Figure S5D). In this line, Treg production of IL-17 was unaffected (Figure S5H).

Tregs with Apc mutations have been repeatedly shown to develop distinct phenotypes with a reduced ability to control the inflammatory response in the pre-cancerous intestine (Chae and Bothwell, 2015; Erdman et al., 2005; Gounaris et al., 2009; Serebrennikova et al., 2012). Evidence for a direct effect of Apc in Treg development has been limited (Chae and Bothwell, 2015) since in Apc^{Min/+} mice the mutation could also affect thymic selection and will alter the intestinal microenvironment. In order to test whether Apc affects Treg phenotype acquisition in a cell-intrinsic manner, we created bone marrow chimeras in which both WT and Apc^{Min/+} T cells developed in the same milieu, competing for individual niches. Interestingly, in these chimeric mice, CD4⁺ T cells of WT origin were much more likely to develop into Foxp3⁺ Tregs in the spleen and lymph nodes as well as the intestinal lamina propria (Figures 6A and 6B). This finding is consistent with the role of NFAT in stabilizing Foxp3 expression. As seen in standard mice, heteroin sufficiency for Apc perturbed the balance between thymic Helios^{bright} natural Tregs (nTregs) and induced ROR γ T⁺ IL-10-producing iTregs, with a notable loss of these iTregs among Apc^{Min/+} cells in the intestine (Figures 6C–6E). Despite developing in exactly the same microenvironment, Tregs arising from Apc^{Min/+} cells exhibited reduced acetylated α -tubulin, particularly after TCR stimulation (Figure 6F), and reduced IL-17 and IL-2 production (Figures S6G and S6H).

These data indicate that disruption of Apc in murine intestinal Foxp3⁺ T cells impairs expression of IL-10 and ROR γ t, and in chimeric mice reduces Treg commitment. This is consistent with impaired NFAT nuclear localization and function, as found in Apc-silenced human T cells.

DISCUSSION

Here, we report a critical role of the polarity regulator APC in TCR signal transduction leading to cytokine gene expression. Importantly, an Apc defect in vivo particularly affects lamina propria Tregs, which display a diminished capacity to produce the anti-inflammatory cytokine IL-10.

We identified APC-regulated microtubule organization as an essential step of NFAT regulation. Importantly, we could visualize NFATC2 microclusters juxtaposed with microtubules. Upon

T cell activation, the distance between NFATC2 microclusters and microtubules increased concomitantly with NFATC2 translocation to the nucleus. Finally, we observed an inhibition of NFAT-driven luciferase gene transcription with colchicine treatment upon T cell activation, consistent with findings from neuroblast cells (Mackenzie and Oteiza, 2007) supporting the importance of microtubules for NFATC2 cellular location. Consistent with a role of microtubules in NFAT translocation to the nucleus, Ishiguro et al., (2011) had shown that NFAT nuclear transport via importin- β required tubulin acetylation. In this line, we suggest that microtubules could facilitate NFAT concentration around the nuclear envelope and facilitate its interaction with nuclear pores. This process would depend on APC-dependent microtubule organization. Few studies have imaged endogenous NFAT in T lymphocytes, and our work reveals a microcluster distribution of NFATC2 that is not observed when overexpressing the GFP-tagged truncated form of NFAT containing the nuclear localization signal and regulatory serine residues. This suggests that the overexpression of GFP-tagged truncated forms of NFAT, while informative, may only partially recapitulate the regulation of endogenous NFAT nuclear translocation. Live imaging of full-length GFP-NFAT appeared particularly challenging since overexpression of this construct was toxic for T cells (S.A.-G., unpublished data).

While APC silencing inhibited NFAT-driven luciferase expression, NF- κ B-driven luciferase remained unaltered and colchicine treatment inhibited both NFAT- and NF- κ B-driven luciferase expression. This is consistent with reported dynein dependence of NF- κ B nuclear translocation (Shrum et al., 2009). In contrast, neither APC silencing nor colchicine altered AP1-driven luciferase (Figures 2C and 2F) (E.V.-C., unpublished data). Therefore, the inhibition of IL2 gene transcription by colchicine is likely due to NFAT and NF- κ B inhibition. Additionally, some effects of colchicine on early TCR signaling, including TCR synaptic clustering, tyrosine phosphorylation and Erk activation were observed before (Das et al., 2004; Lasserre et al., 2010) that could account for the effect of colchicine on TCR-CD28-induced NFAT activation, but would not affect PMA-Iono activation. These data suggest that different microtubule-driven events control NFAT, NF- κ B, and AP1 transcription factor activation. Furthermore, APC silencing may influence IL2 expression through mechanisms other than cytoskeleton reorganization, including reduction of c-Myc and NFAT.

Other proteins use microtubules to translocate from the cytoplasm to the nucleus. Some of them interact with the dynein motor via their nuclear localization signals. Therefore, microtubule-based active transport could bring proteins to nuclear pores,

(D) IL2 mRNA expression assessed by qRT-PCR in human CD4⁺ T cells treated with DMSO or colchicine and activated with PMA/Iono. Data are representative of three experiments (mean \pm SD; Mann-Whitney test).

(E–G) Western blot analysis (E) of NFAT nuclear/cytoplasmic localization of human primary CD4⁺ T cells treated with DMSO or colchicine and activated with anti-CD3+anti-CD28 Abs, lysed, fractionated (ZAP-70 cytoplasmic or histone-3 nuclear controls) and quantified (F and G). Data are representative of three experiments.

(H and I) NFAT protein and mRNA expression in human CD4⁺ T cells (DMSO or colchicine) analyzed by (H) western blot and (I) qRT-PCR. Four (H) and three (I) experiments were performed (mean \pm SD; two-tailed unpaired t test).

(J) Jurkat cells were transfected with expression vectors encoding no gene (empty) or APC-Cter and APC-EB1 schematized on the left. NFAT-driven luciferase expression was analyzed. Data are representative of three experiments (mean \pm SD; one-way ANOVA).

See also Figure S4.

A Nuclear NFAT Treg

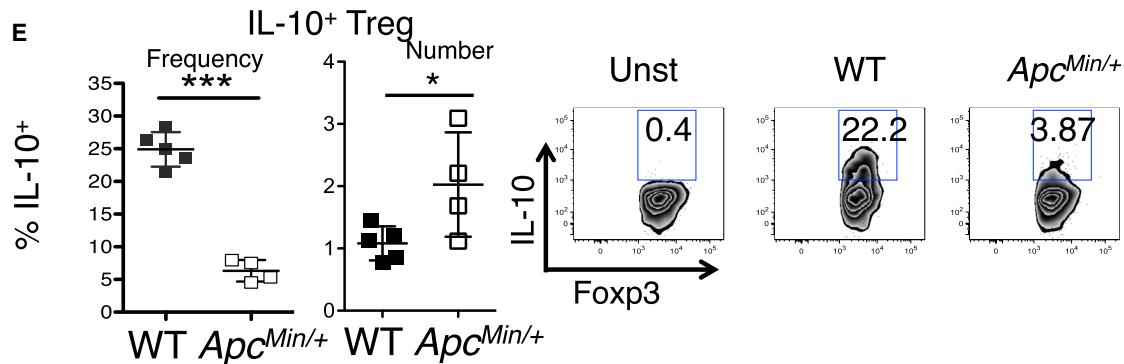
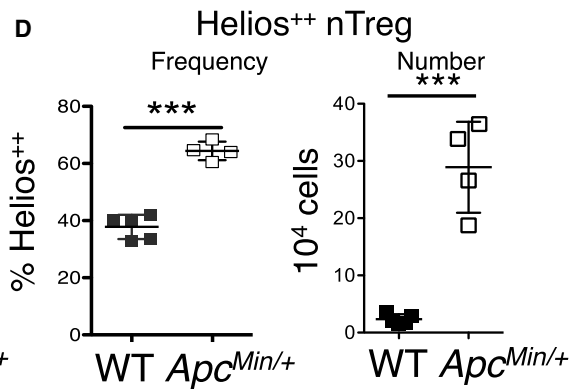
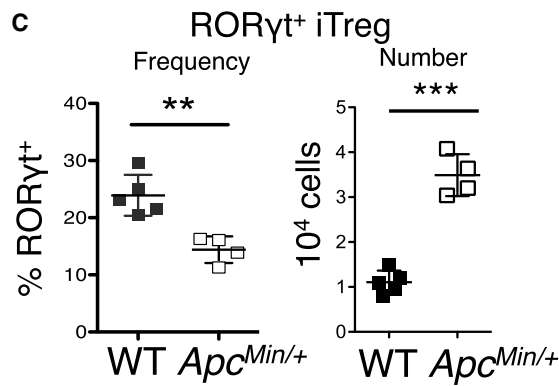
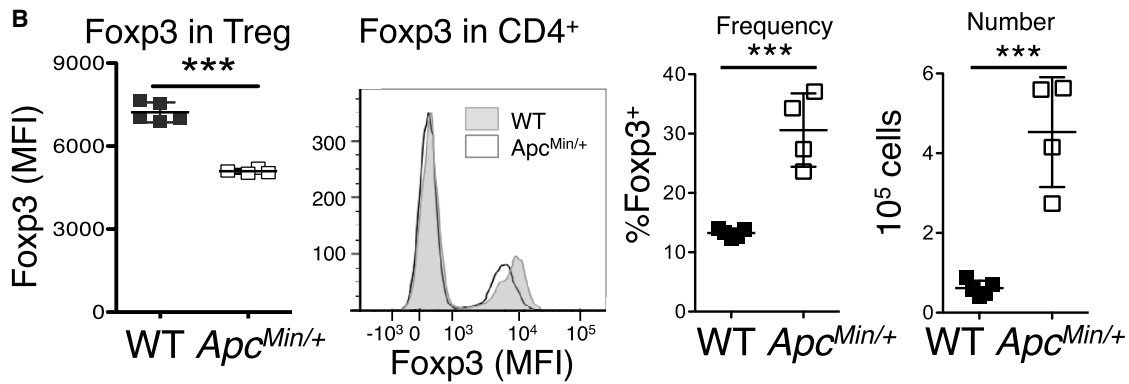
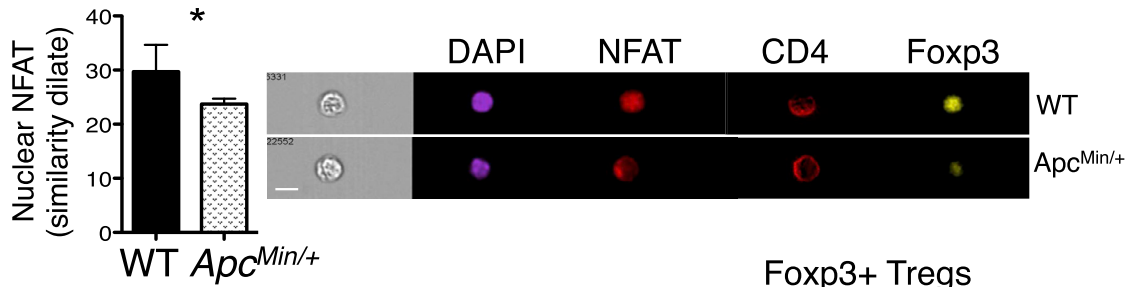


Figure 5. NFAT Nuclear Localization, IL-10 Production, and iTreg Differentiation of Intestinal Tregs in *Apc*^{Min/+} Mutant Mice

(A) Nuclear localization of NFAT in lamina propria Tregs (CD4⁺TCRβ⁺Foxp3⁺) of WT and *Apc*^{Min/+} mice, analyzed by ImageStream (similarity between DAPI and NFAT). Data are representative of two experiments (mean ± SD; two-tailed unpaired t test).

(legend continued on next page)

facilitating interactions with importins and promoting nuclear translocation (Wagstaff and Jans, 2009). Our results here provide further insight into this general process, indicating that a fine microtubule organization controlled by APC is crucial for NFAT transport to the nucleus or NFAT nuclear localization upon T cell activation.

The Wnt/ β -catenin signaling pathway is key for differentiation and growth in various cell systems including thymocytes. APC is part of the β -catenin degradation complex (Stamos and Weis, 2013). APC mutations increase β -catenin cellular levels, deregulating cell differentiation and promoting tumor development in epithelial cells, as well as altered thymocyte development (Gounari et al., 2005; McCartney and Näthke, 2008). β -catenin is a transcription factor that cooperates with T cell factor-1 to coordinate T cell differentiation (Ioannidis et al., 2001). Activation of the TCR leads to β -catenin nuclear stabilization (Lovatt and Bijlmakers, 2010), and a transgenic mouse model of stabilized β -catenin presents reduced LAT and PLC γ phosphorylation and cytokine production (Driessens et al., 2011). In this line, APC-silenced cells could behave as cells expressing stabilized β -catenin. However, we observed that APC-silenced displayed no modification of PLC γ 1 phosphorylation upon TCR activation. In addition, silencing β -catenin was by itself inhibitory for IL2 gene expression and in APC-silenced cells only weakly restored IL2 gene transcription (E.V.-C., unpublished data). This indicates that the effect of APC silencing in T cell activation is unlikely to be entirely due to higher levels of β -catenin.

NFAT cooperates with AP1 and NF- κ B to regulate T cell functions. NFAT-AP1 interaction regulates the balance between T cell proliferation, T cell anergy and exhaustion (Macián et al., 2002; Martinez et al., 2015). Moreover, NFAT regulates Foxp3 expression (Tone et al., 2008) and interacts with Foxp3 to control the transcriptional program of regulatory T cells (Wu et al., 2006). Finally, a fraction of NFAT is constitutively localized in the nucleus of Foxp3⁺ T cells (Li et al., 2012). We found that Apc^{Min/+} intestinal T cells displayed lower levels of total Foxp3 and reduced nuclear NFAT, which together might unbalance cytokine gene transcription. This may explain, at least in part, why Apc^{Min/+} Foxp3⁺ cells produce IL-10 inefficiently. In further agreement with our findings in Apc^{Min/+} mice, Gounaris et al. reported a reduced percentage of intestinal CD4⁺Foxp3⁺ cells that produce IL-10 in Apc Δ^{468} mice. Instead, they found a higher proportion of cells producing IL-17, proposing that a transition toward pro-inflammatory Th17 cells had taken place (Gounaris et al., 2009). However, neither we nor Chae and Bothwell (2015) found an increased percentage of lamina propria IL-17-producing cells in Apc^{Min/+} mice. These discrepancies in the two different experimental mouse models could be due to differences in age, microbiota, or the state of intestinal inflammation in the animals.

Our data showed a higher proportion of Tregs expressing high levels of Helios and low levels of ROR γ t in the lamina propria

from Apc^{Min/+} mice, indicative of a nTreg phenotype. Therefore, Apc mutation impairs CD4⁺ T cell differentiation into, or retention of, the iTreg gene program, particularly in lamina propria Treg, in accordance with previous work (Chae and Bothwell, 2015). At the transcriptional level, iTreg generation could be particularly sensitive to NFAT nuclear levels, as iTreg induction in gut-associated lymphoid tissues is controlled by the non-coding DNA sequence CNS1 at the Foxp3 locus, and CNS1 contains an NFAT-binding site (Zheng et al., 2010). Additionally, our in vitro experiments demonstrate that naive Apc^{Min/+} T cells fail to convert into Foxp3⁺ Tregs under suboptimal TCR stimulation, despite responding similarly to TGF β . This suggests that Apc mutations are most likely to affect Treg generation under suboptimal conditions, such as are likely to occur outside the thymus.

Tregs play a critical role in the control of cancer development in Apc mutant mouse models, as established by experiments in which transfer of WT, but not Apc mutant CD4⁺Foxp3⁺ cells to these mice reduced polyp growth. Moreover, cell-intrinsic loss of a single allele of Apc reduced the ability of Tregs to control cytokine production, and loss of both alleles resulted in a lymphoproliferative wasting phenotype reminiscent of Foxp3 deficiency (Chae and Bothwell, 2015). Therefore, Apc mutant mice appear unable to control cancer-associated intestinal inflammation, as assessed by elevated cytokine transcripts, conversion of T cells to pro-inflammatory phenotypes (IL-17) and increased intestinal mastocytosis (Akeus et al., 2014; Chae and Bothwell, 2015; Gounaris et al., 2007, 2009). Our data are consistent with an intrinsic developmental change in Tregs possibly due to impaired NFAT-driven transcription, including IL-10 (Wu et al., 2006). This intrinsic genetic defect likely acts in concert with other factors in the intestinal microenvironment to result in Treg impairment, as previously suggested by others (Chae and Bothwell, 2015; Peuker et al., 2016).

In sum, we show that the polarity regulator APC modifies NFAT transcriptional activity, and we propose that this phenomenon could be relevant for Treg anti-inflammatory phenotypes in the Apc^{Min/+} mice model of colorectal cancer. We propose that APC could have a dual role in colorectal cancer progression, promoting both epithelial transformation and T lymphocyte dysfunction through suboptimal NFAT regulation.

EXPERIMENTAL PROCEDURES

Antibodies and reagents are described in the [Supplemental Experimental Procedures](#).

Statistical Analysis

Statistical analyses were performed with Prism software (GraphPad). Details about the data presentation, the experimental replication, and the adequate statistical tests used are included in the individual figure legends. Significance symbols are as follows *p < 0.05, ** p < 0.01, *** p < 0.001; ns, non-significant. Mean \pm SD was plotted unless otherwise specified. No data were excluded from the analysis. Experiment sample sizes were selected based on previous

(B–E) Proportional representation and total numbers of small intestinal lamina propria Foxp3⁺ Tregs in WT and Apc^{Min/+} mice. Foxp3 MFI, and Foxp3⁺ Tregs frequency and total number (B). ROR γ T⁺ iTregs (C). Helios^{bright} nTregs (D). IL-10-expressing Tregs (E).

Data are representative of three experiments (mean \pm SD; two-tailed unpaired t test).

See also [Figure S5](#).

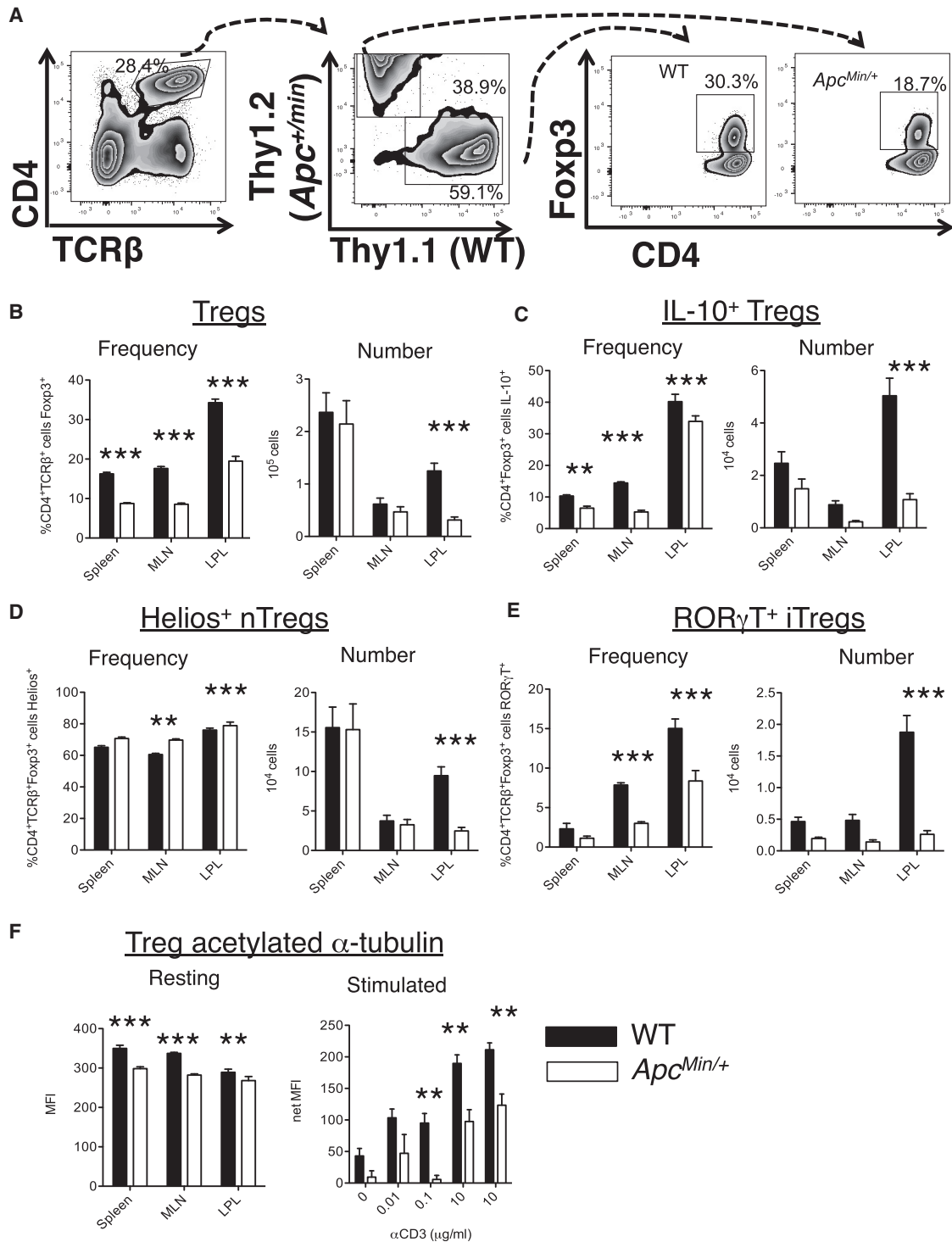


Figure 6. Effect of Apc Mutation on Treg Phenotypes in a Mixed Bone Marrow Chimera

(A) Representative flow cytometry plots showing Foxp3 gating among Thy1.1⁺ WT or Thy1.2⁺ *Apc*^{+/*Min*} cells in the small intestinal lamina propria.

(B) Frequency and total numbers of Foxp3⁺ Tregs among CD4⁺TCRβ⁺ T cells derived from either Thy1.1⁺ WT cells or Thy1.2⁺ *Apc*^{+/*Min*} cells.

(C) Frequency and numbers of IL-10-producing Tregs.

(D) Frequency and numbers of Helios^{bright} nTregs.

(legend continued on next page)

experience with the experimental methods, erring on the larger size. Data met the assumptions of the statistical tests. Sample variance was analyzed for samples > 30 with Prism software. Data were analyzed by observers aware of the sample identities. For selected microscopy experiments, data were examined by a second observer unaware of sample identities. All relevant data are available from the authors.

Cells, siRNA, Cell Culture, and Transfection

Jurkat E6.1 cells (referred to as Jurkat) and Jurkat cells stably expressing YFP-SLP-76 (SLP-76 YFP) have been previously described (Di Bartolo et al., 2007; Lasserre et al., 2011). DLD-1 and HCT-116 human colorectal carcinoma cell lines came from ATCC. Human peripheral blood T cells from healthy volunteers were obtained through the ICAREB core facility at the Institut Pasteur (NSF 96-900 certified, from sampling to distribution, reference BB-0033-00062/ICAREB platform/ Institut Pasteur, Paris, France/BBMRI AO203/ 1 distribution/ access: 2016, May 19th, [BIORESOURCE]), under the CoSImmGen protocol approved by the Committee of Protection of Persons, Ile de France-1 (no. 2010-dec-12483). Informed consent was obtained from all subjects. Isolation of peripheral blood T cells, cell culture methods, and small interfering RNA (siRNA) transfection is described in the [Supplemental Experimental Procedures](#). Isolation of peripheral blood T cells, cell culture methods, and siRNA transfection is described in the [Supplemental Experimental Procedures](#).

Immunofluorescence, Confocal Microscopy, and Image Analysis

Microscopy methods are previously described (Lasserre et al., 2011) and/or detailed in the [Supplemental Experimental Procedures](#).

T Cell Activation

Analyses of protein phosphorylation, tubulin acetylation, intracellular calcium concentration, transcription factor activation by luciferase assays, IL2 and NFAT mRNA measurements by qRT-PCR, and nuclear NFAT detection by cytoplasm/nucleus cell fractionation or by immunofluorescence were performed following the standard methods described in the [Supplemental Experimental Procedures](#).

Apc^{Min/+} Mice, Mesenteric Lymph Node, and Lamina Propria Lymphocyte Isolation

Heterozygous C57BL/6J-Apc^{Min} (Apc^{Min/+}) mice and matched wild-type controls were purchased from the Jackson Laboratory. All mice were bred and maintained under specific pathogen-free barrier conditions. Animal procedures were performed under protocols approved by the Boston Children's Hospital Institutional Animal Care and Use Committee. Animals were sacrificed at 11-12 weeks of age. Females were used. Animals were not randomized. Investigators were not blinded to animal allocation during experiments and outcome assessment.

Generation of mixed bone marrow chimeras, intestinal leukocyte isolation, intracellular cytokine staining, and NFAT nuclear localization in intestinal Tregs by ImageStream flow cytometry was performed following the standard methods described in the [Supplemental Experimental Procedures](#).

SUPPLEMENTAL INFORMATION

Supplemental Information includes Supplemental Experimental Materials, six figures, and seven movies and can be found with this article online at <http://dx.doi.org/10.1016/j.celrep.2017.09.020>.

AUTHOR CONTRIBUTIONS

S.A.-G. designed and performed the experiments, developed the project, and wrote the manuscript; O.T.B. designed and performed the experiments and contributed to manuscript writing; E.V.-C. designed and performed the exper-

iments and assisted in writing the manuscript; C.C. and F.H. performed the experiments, developed the assays, and provided technical support; J.B. and R.L. provided scientific advice; I.d.R.-I. provided expertise and developed the assays; V.d.B. designed and performed experiments, provided expertise, and assisted in writing the manuscript; and A.A. conceived the project, designed the experiments, and wrote the manuscript.

ACKNOWLEDGMENTS

This work was supported by grants from ANR (11BSV302501), The People Programme (Marie Skłodowska-Curie Actions) of the European Union's Seventh Framework Programme (FP7/2007-2013) under a REA grant agreement (no. 317057 HOMIN-ITN), the Institut Pasteur, INSERM, and CNRS (to A.A.) and ARC (PJA-20131200429) (to S.A.-G.). The following fellowships are acknowledged: ARC and ANR postdoctoral fellowships (PDF20101202232 and 11BSV302501 to S.A.-G.); NIDDK K01 career development grant (1K01DK106303-01) (to O.T.B.); ANR (11BSV302501) and Sidaction postdoctoral fellowships (to E.V.-C.); an ANR fellowship (11BSV302501 to F.H.); ANRS (1121/AO2013-2) and Roux-Institut Pasteur postdoctoral fellowships (to J.B.); ANR (11BSV302501), ANRS (1613/CSS1/AO2010-2), and Roux-Institut Pasteur postdoctoral fellowships (to R.L.); and an EU Marie Curie Actions HOMIN-ITN predoctoral fellowship (to I.d.R.-I., who is a scholar in the Pasteur-Paris University [PPU] International PhD program). We thank J.Y. Tinevez, A. Danckaert, P. Roux, A. Salles, E. Perret, and Photonic Biomedicine UTechS, Institut Pasteur for image quantification and technical support and the Cytometry and Biomarkers UTechS, Institut Pasteur for technical support. We are grateful to I. Näthke, I. Newton, M. Bornens, S. Etienne-Manneville, A. Echard, R. Weil, M. Garcia-Gracerá, and M. Almén for plasmids, antibodies, reagents, advice, and statistical analysis, G. Eberl for discussions and critical reading of the manuscript, and the ICAREB team for providing primary T cell samples.

Received: July 20, 2016

Revised: August 4, 2017

Accepted: September 5, 2017

Published: October 3, 2017

REFERENCES

- Agüera-Gonzalez, S., Bouchet, J., and Alcover, A. (2015). Immunological Synapse (John Wiley & Sons). <http://dx.doi.org/10.1002/9780470015902.a0004027.pub2>. <http://onlinelibrary.wiley.com/doi/10.1002/9780470015902.a0004027.pub2/full>.
- Akeus, P., Langenes, V., von Mentzer, A., Yrild, U., Sjöling, Å., Saksena, P., Raghavan, S., and Quiding-Järbrink, M. (2014). Altered chemokine production and accumulation of regulatory T cells in intestinal adenomas of APC(Min/+ mice). *Cancer Immunol. Immunother.* 63, 807–819.
- Beals, C.R., Clipstone, N.A., Ho, S.N., and Crabtree, G.R. (1997a). Nuclear localization of NF-ATc by a calcineurin-dependent, cyclosporin-sensitive intramolecular interaction. *Genes Dev.* 11, 824–834.
- Beals, C.R., Sheridan, C.M., Turck, C.W., Gardner, P., and Crabtree, G.R. (1997b). Nuclear export of NF-ATc enhanced by glycogen synthase kinase-3. *Science* 275, 1930–1934.
- Bérout, C., and Soussi, T. (1996). APC gene: database of germline and somatic mutations in human tumors and cell lines. *Nucleic Acids Res.* 24, 121–124.
- Bertrand, F., Esquerré, M., Petit, A.E., Rodrigues, M., Duchez, S., Delon, J., and Valitutti, S. (2010). Activation of the ancestral polarity regulator protein kinase C zeta at the immunological synapse drives polarization of Th cell secretory machinery toward APCs. *J. Immunol.* 185, 2887–2894.

(E) Frequency and numbers of ROR γ T⁺ iTregs.

(F) Expression of acetylated α -tubulin in freshly isolated Foxp3⁺ Tregs from chimeric mice or after 72 hr stimulation with varying concentrations of α CD3 (splenocytes only). Mean \pm SD, two-way ANOVA with Bonferroni post-tests matching within individual chimeric mice.

See also [Figure S6](#).

- Bunnell, S.C., Hong, D.I., Kardon, J.R., Yamazaki, T., McGlade, C.J., Barr, V.A., and Samelson, L.E. (2002). T cell receptor ligation induces the formation of dynamically regulated signaling assemblies. *J. Cell Biol.* *158*, 1263–1275.
- Campi, G., Varma, R., and Dustin, M.L. (2005). Actin and agonist MHC-peptide complex-dependent T cell receptor microclusters as scaffolds for signaling. *J. Exp. Med.* *202*, 1031–1036.
- Chae, W.J., and Bothwell, A.L. (2015). Spontaneous intestinal tumorigenesis in Apc (Min+) mice requires altered T cell development with IL-17A. *J. Immunol. Res.* *2015*, 860106.
- Chung, A.Y., Li, Q., Blair, S.J., De Jesus, M., Dennis, K.L., LeVeau, C., Yao, J., Sun, Y., Conway, T.F., Virtuoso, L.P., et al. (2014). Oral interleukin-10 alleviates polyposis via neutralization of pathogenic T-regulatory cells. *Cancer Res.* *74*, 5377–5385.
- Das, V., Nal, B., Dujancourt, A., Thoulouze, M.I., Galli, T., Roux, P., Dautry-Varsat, A., and Alcover, A. (2004). Activation-induced polarized recycling targets T cell antigen receptors to the immunological synapse; involvement of SNARE complexes. *Immunity* *20*, 577–588.
- Dennis, K.L., Saadalla, A., Blatner, N.R., Wang, S., Venkateswaran, V., Gounari, F., Cheroutre, H., Weaver, C.T., Roers, A., Egilmez, N.K., and Khazaie, K. (2015). T-cell expression of IL10 is essential for tumor immune surveillance in the small intestine. *Cancer Immunol. Res.* *3*, 806–814.
- Di Bartolo, V., Montagne, B., Salek, M., Jungwirth, B., Carrette, F., Fourtane, J., Sol-Foulon, N., Michel, F., Schwartz, O., Lehmann, W.D., and Acuto, O. (2007). A novel pathway down-modulating T cell activation involves HPK-1-dependent recruitment of 14-3-3 proteins on SLP-76. *J. Exp. Med.* *204*, 681–691.
- Driessens, G., Zheng, Y., Locke, F., Cannon, J.L., Gounari, F., and Gajewski, T.F. (2011). Beta-catenin inhibits T cell activation by selective interference with linker for activation of T cells-phospholipase C- γ 1 phosphorylation. *J. Immunol.* *186*, 784–790.
- Elric, J., and Etienne-Manneville, S. (2014). Centrosome positioning in polarized cells: common themes and variations. *Exp. Cell Res.* *328*, 240–248.
- Erdman, S.E., Sohn, J.J., Rao, V.P., Nambiar, P.R., Ge, Z., Fox, J.G., and Schauer, D.B. (2005). CD4+CD25+ regulatory lymphocytes induce regression of intestinal tumors in ApcMin/+ mice. *Cancer Res.* *65*, 3998–4004.
- Etienne-Manneville, S. (2009). APC in cell migration. *Adv. Exp. Med. Biol.* *656*, 30–40.
- Etienne-Manneville, S., Manneville, J.B., Nicholls, S., Ferenczi, M.A., and Hall, A. (2005). Cdc42 and Par6-PKCzeta regulate the spatially localized association of Dlg1 and APC to control cell polarization. *J. Cell Biol.* *170*, 895–901.
- Gounari, F., Chang, R., Cowan, J., Guo, Z., Dose, M., Gounaris, E., and Khazaie, K. (2005). Loss of adenomatous polyposis coli gene function disrupts thymic development. *Nat. Immunol.* *6*, 800–809.
- Gounaris, E., Erdman, S.E., Restaino, C., Gurish, M.F., Friend, D.S., Gounari, F., Lee, D.M., Zhang, G., Glickman, J.N., Shin, K., et al. (2007). Mast cells are an essential hematopoietic component for polyp development. *Proc. Natl. Acad. Sci. USA* *104*, 19977–19982.
- Gounaris, E., Blatner, N.R., Dennis, K., Magnusson, F., Gurish, M.F., Strom, T.B., Beckhove, P., Gounari, F., and Khazaie, K. (2009). T-regulatory cells shift from a protective anti-inflammatory to a cancer-promoting proinflammatory phenotype in polyposis. *Cancer Res.* *69*, 5490–5497.
- Ioannidis, V., Beermann, F., Clevers, H., and Held, W. (2001). The beta-catenin-TCF-1 pathway ensures CD4(+)CD8(+) thymocyte survival. *Nat. Immunol.* *2*, 691–697.
- Ishiguro, K., Ando, T., Maeda, O., Watanabe, O., and Goto, H. (2011). Cutting edge: tubulin α functions as an adaptor in NFAT-importin β interaction. *J. Immunol.* *186*, 2710–2713.
- Kim, B.G., Li, C., Qiao, W., Mamura, M., Kasprzak, B., Anver, M., Wolfrum, L., Hong, S., Mushinski, E., Potter, M., et al. (2006). Smad4 signalling in T cells is required for suppression of gastrointestinal cancer. *Nature* *441*, 1015–1019.
- Kroboth, K., Newton, I.P., Kita, K., Dikovskaya, D., Zumbunn, J., Waterman-Storer, C.M., and Näthke, I.S. (2007). Lack of adenomatous polyposis coli protein correlates with a decrease in cell migration and overall changes in microtubule stability. *Mol. Biol. Cell* *18*, 910–918.
- Lasserre, R., Charrin, S., Cucho, C., Danckaert, A., Thoulouze, M.I., de Chaudmont, F., Duong, T., Perrault, N., Varin-Blank, N., Olivo-Marin, J.C., et al. (2010). Ezrin tunes T-cell activation by controlling Dlg1 and microtubule positioning at the immunological synapse. *EMBO J.* *29*, 2301–2314.
- Lasserre, R., Cucho, C., Blecher-Gonen, R., Libman, E., Biquand, E., Danckaert, A., Yablonski, D., Alcover, A., and Di Bartolo, V. (2011). Release of serine/threonine-phosphorylated adaptors from signaling microclusters down-regulates T cell activation. *J. Cell Biol.* *195*, 839–853.
- Li, Q., Shakya, A., Guo, X., Zhang, H., Tantin, D., Jensen, P.E., and Chen, X. (2012). Constitutive nuclear localization of NFAT in Foxp3+ regulatory T cells independent of calcineurin activity. *J. Immunol.* *188*, 4268–4277.
- Lochner, M., Peduto, L., Cherrier, M., Sawa, S., Langa, F., Varona, R., Riethmacher, D., Si-Tahar, M., Di Santo, J.P., and Eberl, G. (2008). In vivo equilibrium of proinflammatory IL-17+ and regulatory IL-10+ Foxp3+ RORgamma t+ T cells. *J. Exp. Med.* *205*, 1381–1393.
- Lovatt, M., and Bijlmakers, M.J. (2010). Stabilisation of β -catenin downstream of T cell receptor signalling. *PLoS ONE* *5*, 5.
- Ludford-Menting, M.J., Oliaro, J., Sacirbegovic, F., Cheah, E.T., Pedersen, N., Thomas, S.J., Pasam, A., Iazzolino, R., Dow, L.E., Waterhouse, N.J., et al. (2005). A network of PDZ-containing proteins regulates T cell polarity and morphology during migration and immunological synapse formation. *Immunity* *22*, 737–748.
- Macián, F., García-Cózar, F., Im, S.H., Horton, H.F., Byrne, M.C., and Rao, A. (2002). Transcriptional mechanisms underlying lymphocyte tolerance. *Cell* *109*, 719–731.
- Mackenzie, G.G., and Oteiza, P.I. (2007). Zinc and the cytoskeleton in the neuronal modulation of transcription factor NFAT. *J. Cell. Physiol.* *210*, 246–256.
- Martinez, G.J., Pereira, R.M., Äijö, T., Kim, E.Y., Marangoni, F., Pipkin, M.E., Togher, S., Heissmeyer, V., Zhang, Y.C., Crotty, S., et al. (2015). The transcription factor NFAT promotes exhaustion of activated CD8^T T cells. *Immunity* *42*, 265–278.
- McCartney, B.M., and Näthke, I.S. (2008). Cell regulation by the Apc protein Apc as master regulator of epithelia. *Curr. Opin. Cell Biol.* *20*, 186–193.
- Mogensen, M.M., Tucker, J.B., Mackie, J.B., Prescott, A.R., and Näthke, I.S. (2002). The adenomatous polyposis coli protein unambiguously localizes to microtubule plus ends and is involved in establishing parallel arrays of microtubule bundles in highly polarized epithelial cells. *J. Cell Biol.* *157*, 1041–1048.
- Moser, A.R., Pitot, H.C., and Dove, W.F. (1990). A dominant mutation that predisposes to multiple intestinal neoplasia in the mouse. *Science* *247*, 322–324.
- Näthke, I.S., Adams, C.L., Polakis, P., Sellin, J.H., and Nelson, W.J. (1996). The adenomatous polyposis coli tumor suppressor protein localizes to plasma membrane sites involved in active cell migration. *J. Cell Biol.* *134*, 165–179.
- Nelson, S., and Näthke, I.S. (2013). Interactions and functions of the adenomatous polyposis coli (APC) protein at a glance. *J. Cell Sci.* *126*, 873–877.
- Ohnmacht, C., Park, J.H., Cording, S., Wing, J.B., Atarashi, K., Obata, Y., Gaboriau-Routhiau, V., Marques, R., Dulauroy, S., Fedoseeva, M., et al. (2015). Mucosal immunology. The microbiota regulates type 2 immunity through ROR γ t(+) T cells. *Science* *349*, 989–993.
- Okamura, H., Aramburu, J., García-Rodríguez, C., Viola, J.P., Raghavan, A., Tahiliani, M., Zhang, X., Qin, J., Hogan, P.G., and Rao, A. (2000). Concerted dephosphorylation of the transcription factor NFAT1 induces a conformational switch that regulates transcriptional activity. *Mol. Cell* *6*, 539–550.
- Peuker, K., Muff, S., Wang, J., Künzel, S., Bosse, E., Zeissig, Y., Luzzi, G., Basic, M., Strigli, A., Ulbricht, A., et al. (2016). Epithelial calcineurin controls microbiota-dependent intestinal tumor development. *Nat. Med.* *22*, 506–515.
- Real, E., Faure, S., Donnadieu, E., and Delon, J. (2007). Cutting edge: atypical PKCs regulate T lymphocyte polarity and scanning behavior. *J. Immunol.* *179*, 5649–5652.
- Rodríguez-Boulan, E., and Macara, I.G. (2014). Organization and execution of the epithelial polarity programme. *Nat. Rev. Mol. Cell Biol.* *15*, 225–242.

- Round, J.L., Humphries, L.A., Tomassian, T., Mittelstadt, P., Zhang, M., and Miceli, M.C. (2007). Scaffold protein Dlg1 coordinates alternative p38 kinase activation, directing T cell receptor signals toward NFAT but not NF-kappaB transcription factors. *Nat. Immunol.* **8**, 154–161.
- Rubtsov, Y.P., Rasmussen, J.P., Chi, E.Y., Fontenot, J., Castelli, L., Ye, X., Treuting, P., Siewe, L., Roers, A., Henderson, W.R., Jr., et al. (2008). Regulatory T cell-derived interleukin-10 limits inflammation at environmental interfaces. *Immunity* **28**, 546–558.
- Serebrennikova, O.B., Tsatsanis, C., Mao, C., Gounaris, E., Ren, W., Siracusa, L.D., Eliopoulos, A.G., Khazaie, K., and Tscholis, P.N. (2012). Tpl2 ablation promotes intestinal inflammation and tumorigenesis in *Apc*min mice by inhibiting IL-10 secretion and regulatory T-cell generation. *Proc. Natl. Acad. Sci. USA* **109**, E1082–E1091.
- Sharma, S., Findlay, G.M., Bandukwala, H.S., Oberdoerffer, S., Baust, B., Li, Z., Schmidt, V., Hogan, P.G., Sacks, D.B., and Rao, A. (2011). Dephosphorylation of the nuclear factor of activated T cells (NFAT) transcription factor is regulated by an RNA-protein scaffold complex. *Proc. Natl. Acad. Sci. USA* **108**, 11381–11386.
- Shibasaki, F., Price, E.R., Milan, D., and McKeon, F. (1996). Role of kinases and the phosphatase calcineurin in the nuclear shuttling of transcription factor NF-AT4. *Nature* **382**, 370–373.
- Shrum, C.K., Defrancisco, D., and Meffert, M.K. (2009). Stimulated nuclear translocation of NF-kappaB and shuttling differentially depend on dynein and the dynactin complex. *Proc. Natl. Acad. Sci. USA* **106**, 2647–2652.
- Soares, H., Lasserre, R., and Alcover, A. (2013). Orchestrating cytoskeleton and intracellular vesicle traffic to build functional immunological synapses. *Immunol. Rev.* **256**, 118–132.
- Stamos, J.L., and Weis, W.I. (2013). The β -catenin destruction complex. *Cold Spring Harb. Perspect. Biol.* **5**, a007898.
- Su, L.K., Kinzler, K.W., Vogelstein, B., Preisinger, A.C., Moser, A.R., Luongo, C., Gould, K.A., and Dove, W.F. (1992). Multiple intestinal neoplasia caused by a mutation in the murine homolog of the APC gene. *Science* **256**, 668–670.
- Tanner, S.M., Daft, J.G., Hill, S.A., Martin, C.A., and Lorenz, R.G. (2016). Altered T-cell balance in lymphoid organs of a mouse model of colorectal cancer. *J. Histochem. Cytochem.* **64**, 753–767.
- Tone, Y., Furuuchi, K., Kojima, Y., Tykocinski, M.L., Greene, M.I., and Tone, M. (2008). Smad3 and NFAT cooperate to induce Foxp3 expression through its enhancer. *Nat. Immunol.* **9**, 194–202.
- Vaeth, M., Schliesser, U., Müller, G., Reissig, S., Satoh, K., Tuetttenberg, A., Jonuleit, H., Waisman, A., Müller, M.R., Serfling, E., et al. (2012). Dependence on nuclear factor of activated T-cells (NFAT) levels discriminates conventional T cells from Foxp3+ regulatory T cells. *Proc. Natl. Acad. Sci. USA* **109**, 16258–16263.
- van der Veeken, J., Arvey, A., and Rudensky, A. (2013). Transcriptional control of regulatory T-cell differentiation. *Cold Spring Harb. Symp. Quant. Biol.* **78**, 215–222.
- Wagstaff, K.M., and Jans, D.A. (2009). Importins and beyond: non-conventional nuclear transport mechanisms. *Traffic* **10**, 1188–1198.
- Wu, Y., Borde, M., Heissmeyer, V., Feuerer, M., Lapan, A.D., Stroud, J.C., Bates, D.L., Guo, L., Han, A., Ziegler, S.F., et al. (2006). FOXP3 controls regulatory T cell function through cooperation with NFAT. *Cell* **126**, 375–387.
- Xavier, R., Rabizadeh, S., Ishiguro, K., Andre, N., Ortiz, J.B., Wachtel, H., Morris, D.G., Lopez-Illasaca, M., Shaw, A.C., Swat, W., and Seed, B. (2004). Discs large (Dlg1) complexes in lymphocyte activation. *J. Cell Biol.* **166**, 173–178.
- Yang, B.H., Hagemann, S., Mamareli, P., Lauer, U., Hoffmann, U., Beckstette, M., Föhse, L., Prinz, I., Pezoldt, J., Suerbaum, S., et al. (2016). Foxp3(+) T cells expressing ROR γ t represent a stable regulatory T-cell effector lineage with enhanced suppressive capacity during intestinal inflammation. *Mucosal Immunol.* **9**, 444–457.
- Yokosuka, T., Sakata-Sogawa, K., Kobayashi, W., Hiroshima, M., Hashimoto-Tane, A., Tokunaga, M., Dustin, M.L., and Saito, T. (2005). Newly generated T cell receptor microclusters initiate and sustain T cell activation by recruitment of Zap70 and SLP-76. *Nat. Immunol.* **6**, 1253–1262.
- Zeineldin, M., and Neufeld, K.L. (2013). More than two decades of *Apc* modeling in rodents. *Biochim. Biophys. Acta* **1836**, 80–89.
- Zheng, Y., Josefowicz, S., Chaudhry, A., Peng, X.P., Forbush, K., and Rudensky, A.Y. (2010). Role of conserved non-coding DNA elements in the Foxp3 gene in regulatory T-cell fate. *Nature* **463**, 808–812.

Cell Reports, Volume 21

Supplemental Information

**Adenomatous Polyposis Coli Defines Treg
Differentiation and Anti-inflammatory Function
through Microtubule-Mediated NFAT Localization**

Sonia Agüera-González, Oliver T. Burton, Elena Vázquez-Chávez, Céline Cuche, Floriane Herit, Jérôme Bouchet, Rémi Lasserre, Iratxe del Río-Iñiguez, Vincenzo Di Bartolo, and Andrés Alcover

Supplemental Information
Supplemental Figures and Legends

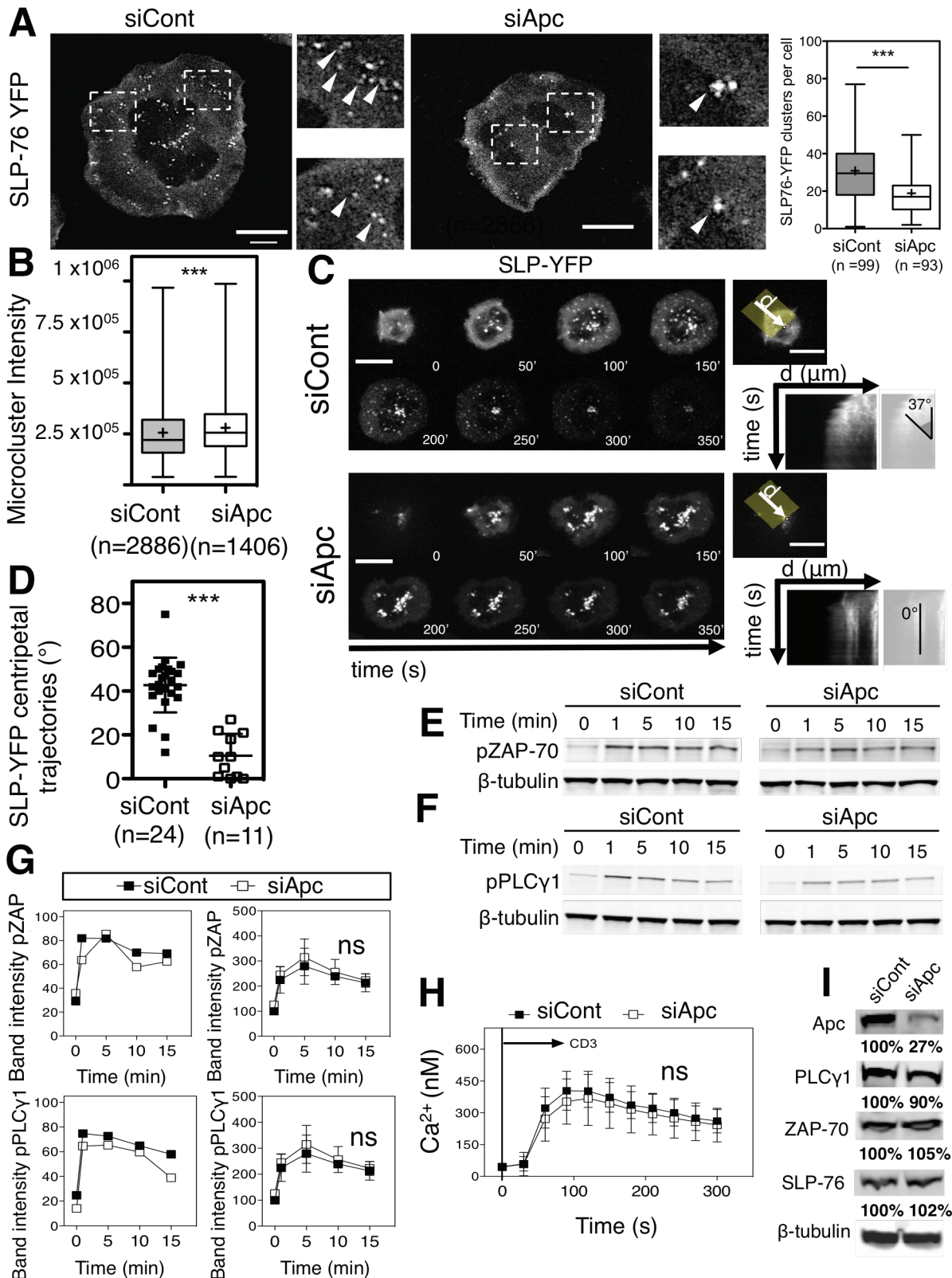


Figure S1 (linked to Figure 1): Effect of APC silencing in early T cell activation events.

A) Generation of SLP76-YFP microclusters in siCont and siApc Jurkat cells on pseudospines (anti-CD3-coated coverslips, 3 min). Framed regions are zoomed on the right panels. Graph represents number of microclusters per cell (whiskers: min-max, +: mean). Representative experiment of three (mean±SD, Mann-Whitney). Scale bar 3 μm. **B**) Intensity of SLP76 YFP microclusters (whiskers: min-max, +: mean). Representative experiment of two (mean±SD, Mann-Whitney). **C, D**) Dynamics of SLP76-YFP microclusters. Kymographs of centripetal microcluster movement were generated and trajectory angles were measured. Representative of two (mean±SD, Mann-Whitney). **E-G**) Tyr phosphorylation of proximal TCR signaling molecules in siCont and siApc Jurkat cells activated with soluble anti-CD3+CD28 Abs, p-ZAP70, Tyr319 (**E**) and p-PLCγ1, Tyr783 (**F**). **E, F**) Blots of one representative experiment. **G Left**) Band intensity (normalized to β-tubulin) of experiment shown. **G Right**) Mean±SD of three experiments, 2-way ANOVA. **H**) Intracellular calcium concentration. Jurkat cells (siCont or siApc) were loaded with the Ca²⁺ sensor Fluo3-AM and activated with soluble anti-CD3 Ab. Intracellular Ca²⁺ concentration was calculated as previously described (Kao et al., 1989) (mean±SD of seven experiments, 2-way ANOVA). **I**) SLP-76, PLCγ1 or ZAP-70 expression.

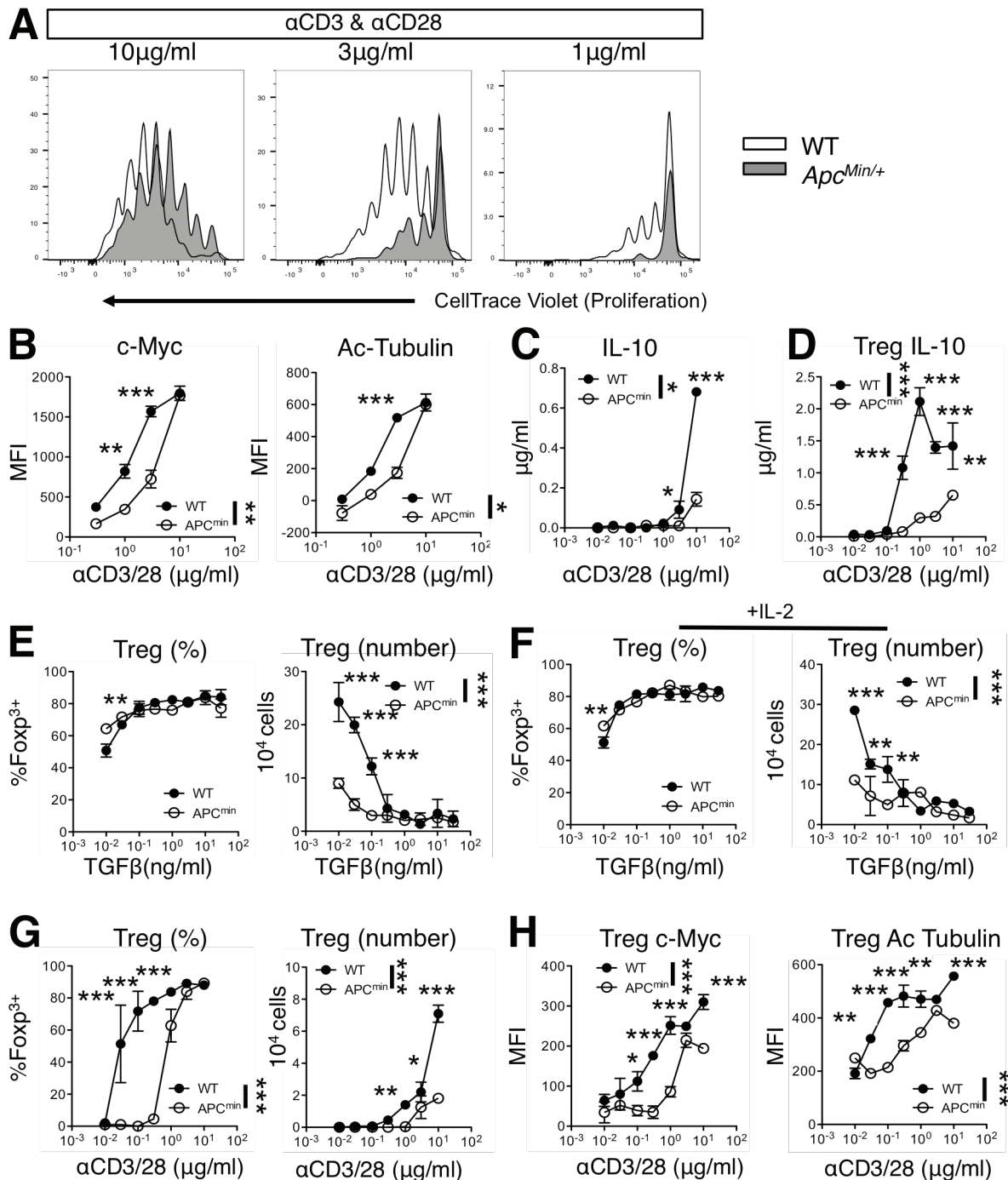


Figure S2 (linked to Figure 2): Impact of heterozygous *Apc* mutation on T cell activation and differentiation *in vitro*.

A) Representative flow histograms showing dye dilution in proliferating CD4⁺ T cells after 72h stimulation with varying concentrations of anti-CD3+CD28. **B)** Analysis of c-Myc and acetylated α -tubulin in CD4⁺ T cells following activation with anti-CD3+CD28. **C)** ELISA analysis of secreted IL-10. **D)** ELISA analysis of IL-10 secreted by WT and *Apc^{+Min}* T cells under Foxp3-inducing conditions. **E)** Impact of heterozygous *Apc* mutation on Foxp3 induction in naïve T cells *in vitro*. Foxp3⁺ T cells induced under varying concentrations of TGF β . Frequencies and total numbers of Foxp3⁺ T cells recovered are shown. **F)** Foxp3⁺ T cells induced under varying concentrations of TGF β in the presence of IL-2 (5ng/ml). **G)** Foxp3⁺ T cells induced in response to varying concentrations of anti-CD3 + CD28. **H)** c-Myc and acetylated α -tubulin expression in Foxp3⁺ T cells generated in responses to variable TCR stimulation. Data are presented as the mean \pm SD of triplicate cultures, and are representative of two independent experiments. Statistical analysis by 2-way ANOVA with Bonferroni post-tests for individual concentrations.

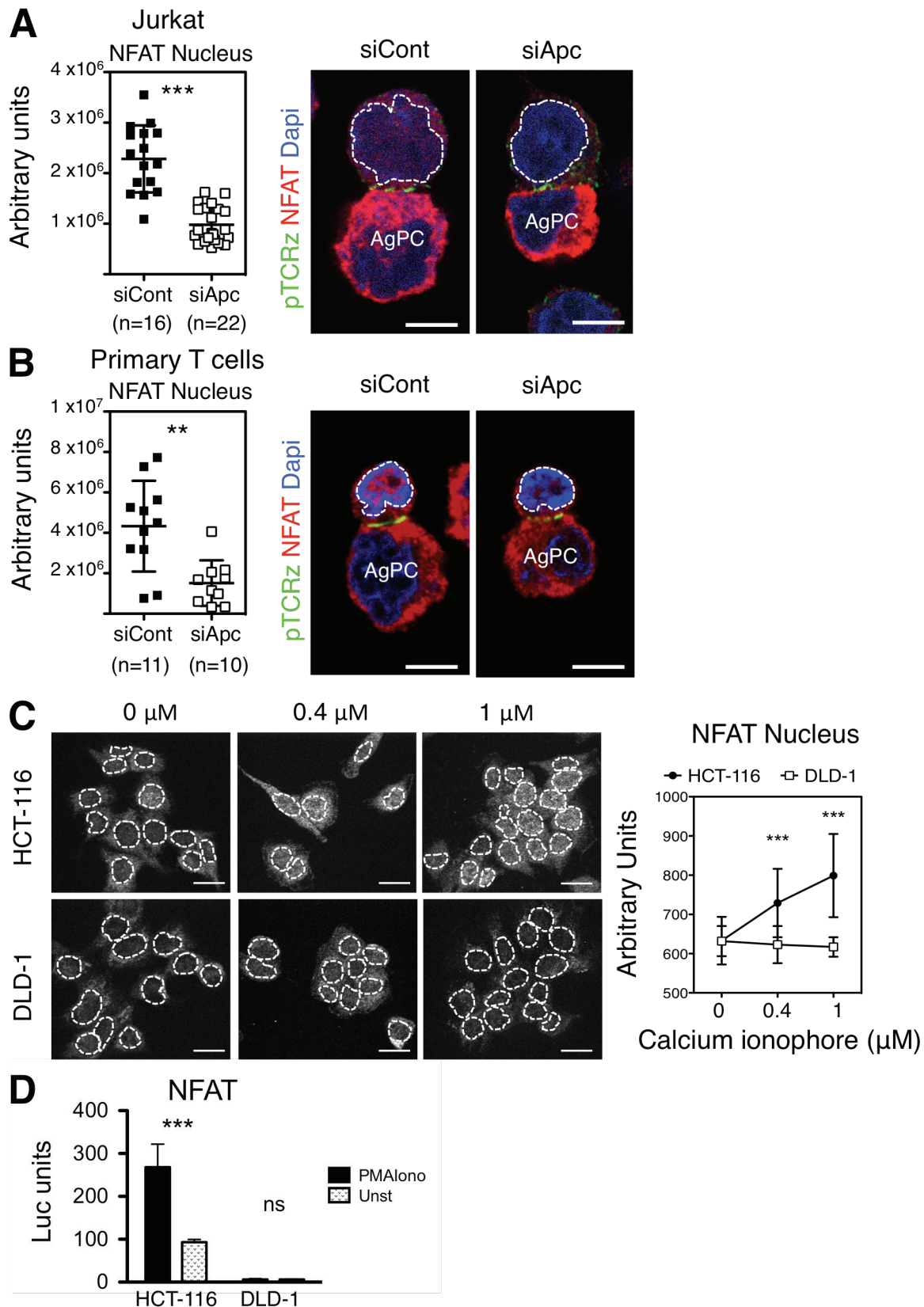


Figure S3 (linked to F2): Effect of APC silencing or APC truncation on NFAT nuclear translocation and NFAT-driven transcription.

A, B NFATc2 nuclear localization in Jurkat (**A**), or human primary CD4⁺ T cells (**B**), activated with SEE-loaded Raji cells as antigen presenting cells. Immunological synapses were scored using p-TCR ζ staining. Representative of three experiments in **A** and two in **B** (mean \pm SD Mann-Whitney). Scale bar 5 μ m. **C** HCT-116 and DLD-1 colon carcinoma cells expressing full-length or truncated APC, respectively, were activated with 10 ng/ml PMA and increased concentrations of calcium ionophore (5 min). NFATc2 nuclear localization was measured using a mask based on Dapi nuclear staining. Representative of two experiments. (mean \pm SD Mann-Whitney test). Scale bar 5 μ m. **D** HCT-116 and DLD-1 carcinoma cells were analyzed for their capacity to activate NFAT-driven luciferase in response to PMA-Iono activation. Average of three experiments (mean \pm SD, 2-way ANOVA).

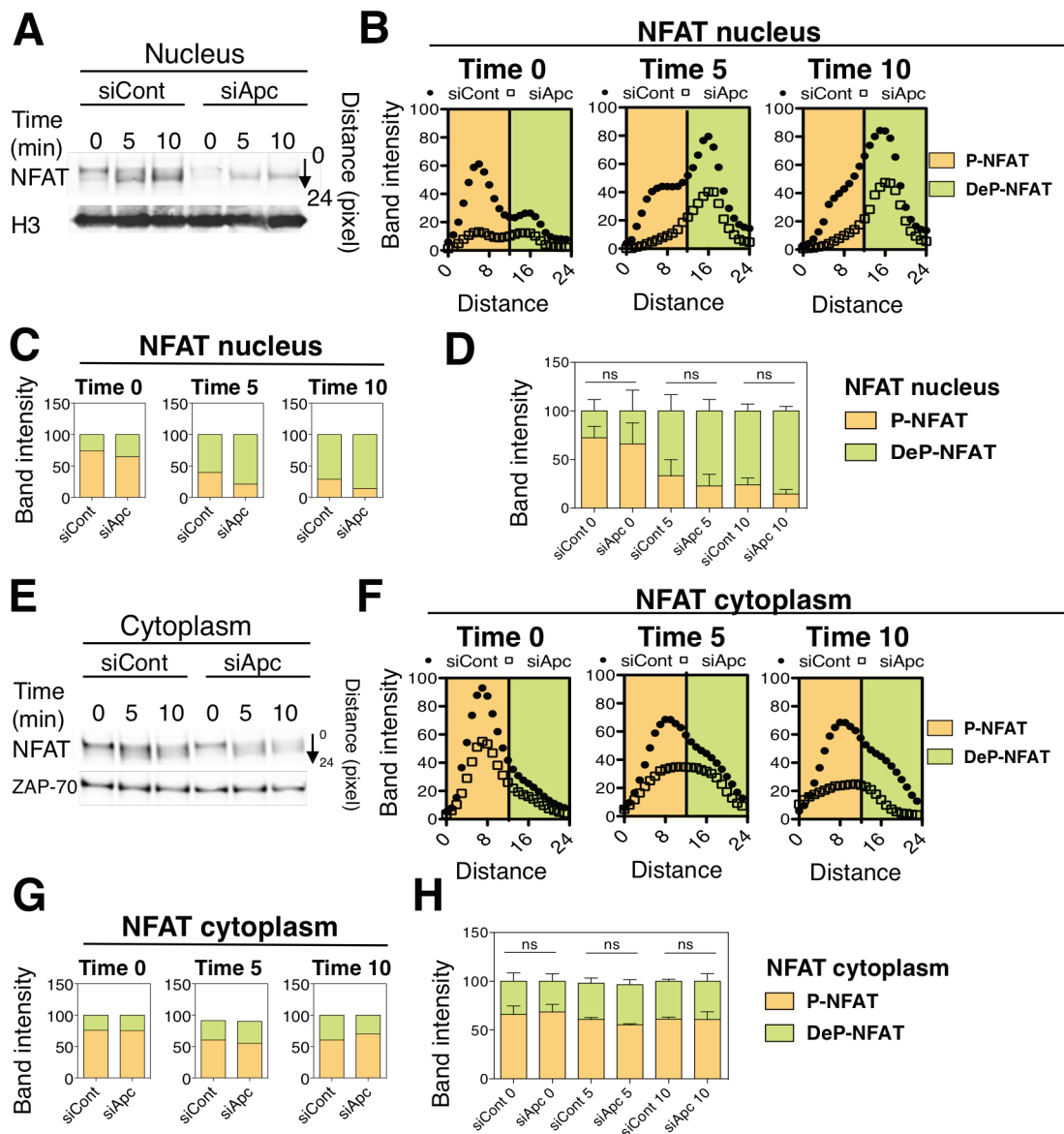


Figure S4 (linked to F2): APC silencing does not alter NFAT dephosphorylation upon T cell activation. Jurkat cells were processed as in Fig. 2J. Densitometry of NFATC2 western blot bands was performed for a distance of 24 pixels (arrow on the right side). **A, E**) Nuclear and cytoplasmic NFATC2 western blots. **B, F**) Densitometry histograms of nuclear and cytoplasmic NFATC2 bands revealing higher bands corresponding to phospho-NFAT (P-NFAT, orange) and lower bands corresponding to dephospho-NFAT (DeP-NFAT, green). **C, G**) Quantification of histograms in panels B and F, respectively. **D, H**) Quantification of three experiments (mean \pm SD, 2-way ANOVA).

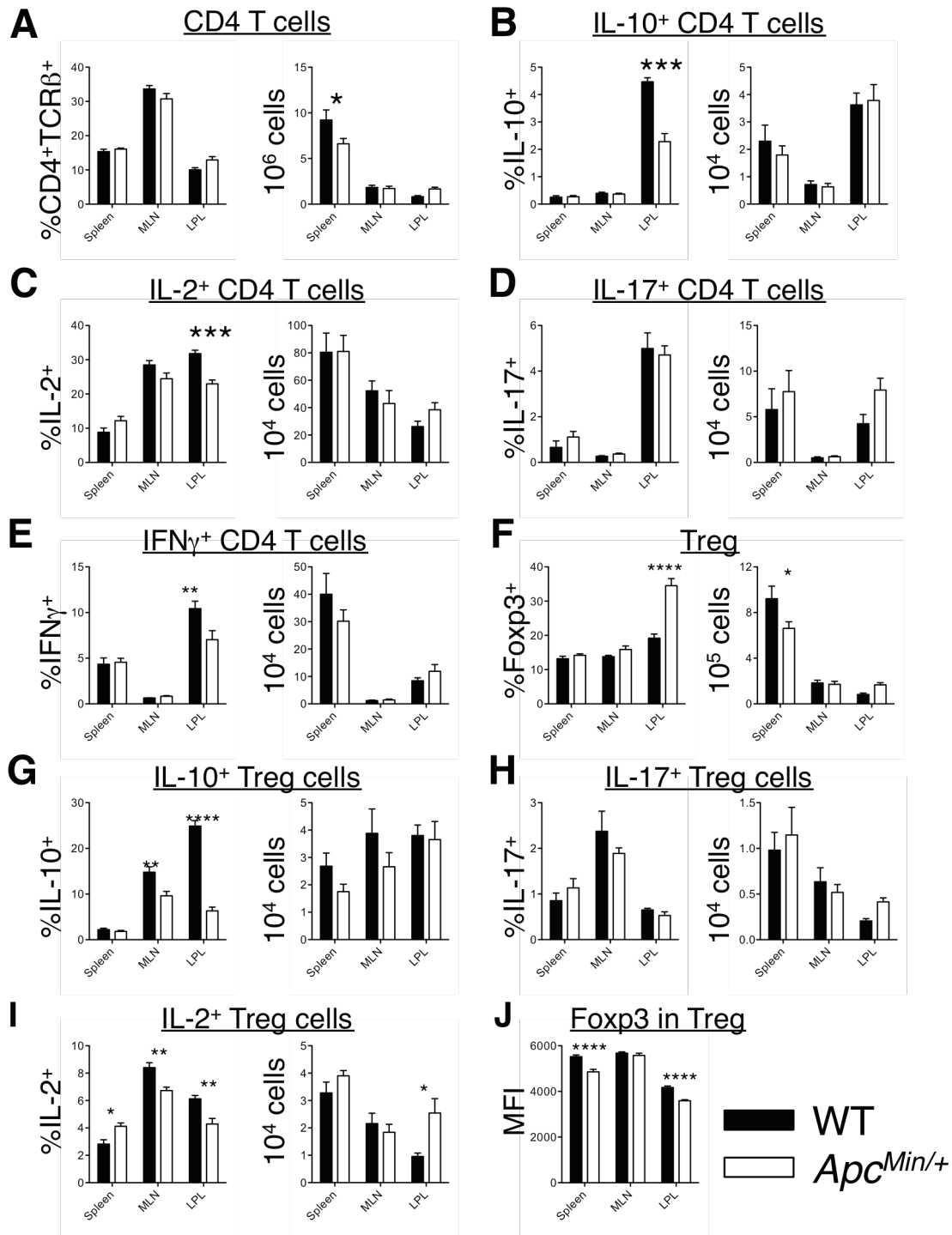


Figure S5 (linked to F5): Impact of heterozygous *Apc* mutation on frequencies and total numbers of cytokine-producing T helper subsets.

A) Percentages and total numbers of CD4⁺TCRβ⁺ cells WT vs. *Apc*^{Min/+} mice. B) IL-10-expressing T cells. C) IL-2-producing T cells. D) Th17 cells. E) IFNγ⁺ cells. F) Tregs. G) IL-10⁺ Treg. H) IL-17⁺ Treg. I) IL-2⁺ Treg. J) Level of Foxp3 expression within Foxp3⁺ cells. Representative of two experiments. Mean±SD. Statistical analysis by 2-way ANOVA with Bonferroni post-tests for individual organs.

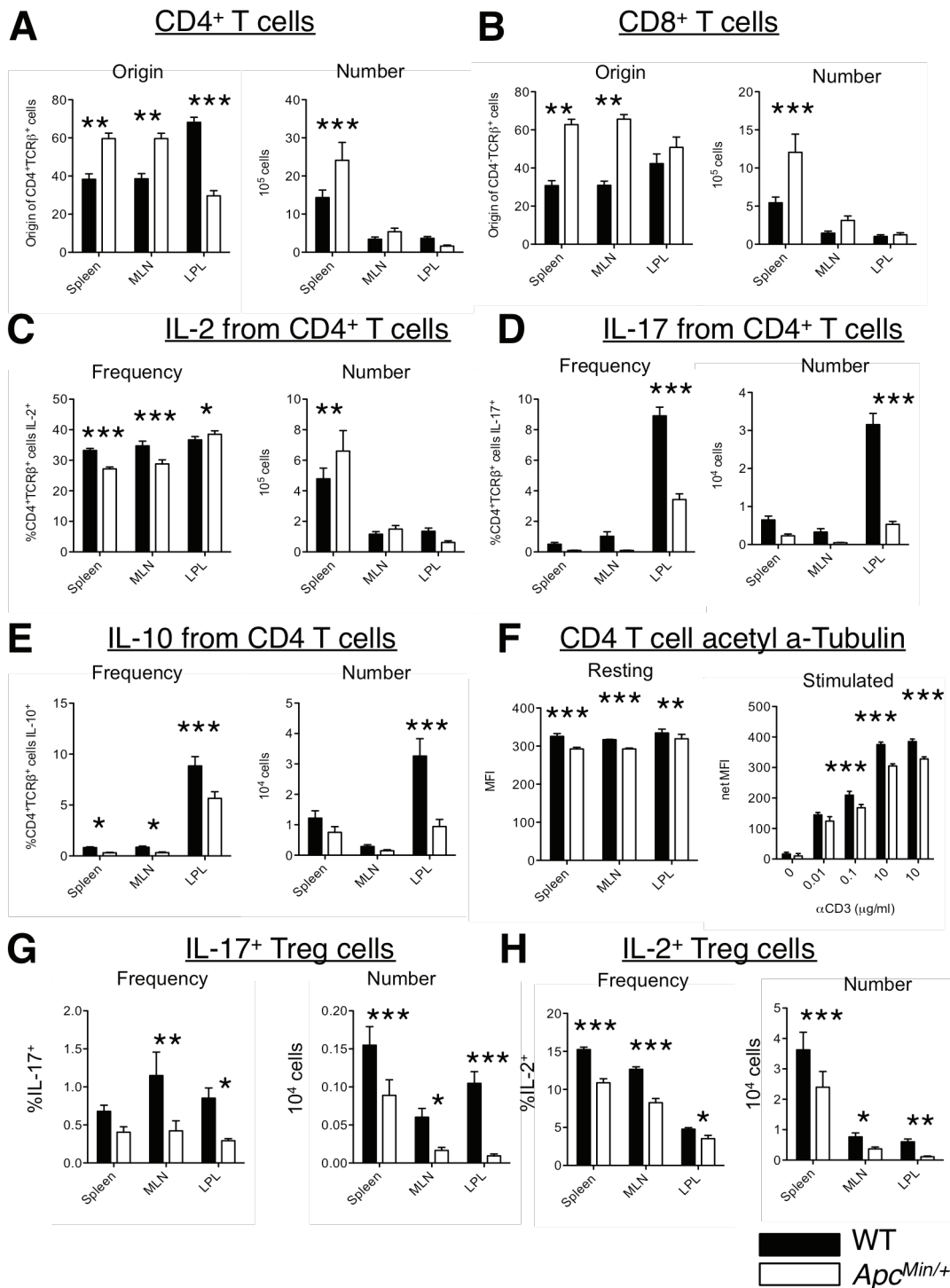


Figure S6 (linked to F6): Cell-intrinsic effect of *Apc* mutation on T cell phenotypes in a mixed bone marrow chimera.

A) Origin (Thy1.1⁺ WT or Thy1.2⁺ *Apc*^{Min/+}) and total numbers of CD4⁺TCRβ⁺ T cells in mixed bone marrow chimerae. **B**) Origin and numbers of CD4⁺TCRβ⁺ (CD8) T cells. **C**) Frequency of IL-2 production among WT or *Apc*^{Min/+} CD4⁺ T cells, and total numbers of IL-2⁺ cells of each type. **D**) Frequency and numbers of IL-17⁺ CD4 T cells. **E**) Frequency and numbers of IL-10⁺ CD4 T cells. **F**) Expression of acetylated α-tubulin in freshly isolated CD4 T cells from chimeric mice, or after 72 h stimulation with varying concentrations of anti-CD3 (splenocytes only). **G**) Frequency and total numbers of IL-17-producing cells among Foxp3⁺ cells of Thy1.1⁺ WT or Thy1.2⁺ *Apc*^{Min/+} origin in mixed bone marrow chimerae. **H**) Frequency and numbers of IL-2⁺ Treg. Mean±SD, statistical analysis by repeated measures 2-way ANOVA with Bonferroni post-tests matching within individual chimeric mice.

Supplemental videos

Movie S1: 3D reconstruction of confocal microscopy images of APC (Red) and microtubules (Green) of Figure 1C. Jurkat cells were activated for 3 min on anti-CD3-coated coverslips, fixed, stained for anti- β -tubulin (green) and anti-APC (red).

Movie S2: 3D segmentation of NFAT clusters (Colored dots) and microtubules (Green) of Figure 3B (Unstimulated cells). NFAT clusters were colored ranging from violet to red according to their distance to the closest microtubule (colored scale).

Movie S3: 3D segmentation of NFAT clusters (Colored dots) and microtubules (Green) of Figure 3C (4 minutes stimulation).

Movie S4: 3D segmentation of NFAT clusters (Colored dots) and microtubules (Green) of Figure 3C (8 minutes stimulation).

Movie S5: 3D segmentation of NFAT clusters (Colored dots) and microtubules (Green) of Figure 3C (20 minutes stimulation).

Video S6: Microcluster dynamics in siCont SLP-YFP Jurkat cells stimulated on anti-CD3-coated coverslips.

Video S7: Microcluster dynamics in siAPC SLP-YFP Jurkat cells stimulated on anti-CD3-coated coverslips.

Supplemental Experimental Procedures

Materials

Antibodies

Antibodies used for western blots: mouse IgG1 anti-APC (N-terminal) (Ali-12-28, Abcam) at 1 μ g/ml, mouse anti- β -tubulin (Sigma) at 1/1000, mouse anti-acetylated-tubulin (Ac-tubulin) (Lys⁴⁰, clone 6-11B-1, Sigma) at 0.6 μ g/ml, rabbit anti-phospho-ZAP-70 (pY319) (Cell Signaling) at 1/1000, rabbit anti-phospho-PLC γ 1 (Tyr783) (Cell Signaling) at 1/1000, rabbit anti-ZAP-70 (Becton Dickinson) at 1/1000, rabbit anti-PLC γ 1 (Cell Signaling) at 1/1000, rabbit anti-SLP76 (ThermoFisher Scientific) at 1/1000, rabbit anti-NFAT1 (Cell Signaling) at 1/1000 and rabbit anti-histone-3 (H3) (Abcam) at 1 μ g/ml.

Antibodies used for immunofluorescence: rabbit anti-APC (gift of I. Näthke, University of Dundee) at 1/500, mouse IgG2b anti- β -tubulin (clone KMX-1, Millipore) at 10 μ g/ml, rabbit anti-centrin (gift of M. Bornens, Institut Curie) at 1/400, mouse IgG1 anti-NFAT (BD Biosciences) and rabbit anti-NFAT1 (Cell Signaling) at 1/150. Secondary antibodies were: goat anti-rabbit IgG-Cy3 (Jackson ImmunoResearch), goat anti-rabbit-FITC (Jackson ImmunoResearch), goat anti-mouse IgG2b-FITC (Southern Biotech), goat anti-mouse IgG2b-Cy3 (Jackson ImmunoResearch), goat anti-mouse IgG1-FITC (Southern Biotech), goat anti-mouse IgG1-Cy3 (Jackson ImmunoResearch) and goat anti-FITC-Alexa 488 (Molecular Probes), all used at 1/100.

Antibodies for activation experiments: mouse IgM anti-CD3 (MEM92, Interchim) at 10 μ g/ml, mouse IgG1 anti-CD28 (Affimetrix, eBioscience) 10 μ g/ml were used for Jurkat cells. Mouse IgM anti-CD3-biotin (Sigma) at 10 μ g/ml, mouse IgG1 anti-CD28-biotin at 10 μ g/ml (Sigma) were used for primary human CD4⁺ T cells. Mouse IgG1 anti-CD3 (UHCT1, Biolegend) 10 μ g/ml was used for calcium experiments. Mouse IgM anti-CD3 (MEM92, Interchim) at 10 μ g/ml was used for coating coverslips for experiments of pseudosynapses.

Antibodies for mouse lymphocyte staining for flow cytometry analysis: anti-CD45-Alexa Fluor-700 (clone 30-F11, Biolegend) at 1/200, anti-CD4-Brilliant Violet-605 (RM4-5, Biolegend) at 1/200, anti-TCRb-PE-Cy7 (H57-597, Biolegend) at 1/100, anti-Foxp3-APC (clone FJK-16s, eBioscience) at 1/100, anti-Foxp3-PE (clone FJK-16s, eBioscience) at 1/100, anti-IL-17-PerCP-Cy5.5 (TC11-18H10.1, Biolegend) at 1/500, anti-IL-2-PE (JES6-5H4, Biolegend) at 1/300, anti-IL-10-Brilliant Violet-421 (JES5-16E3, Biolegend) at 1/300, anti-RORgt-PE-eFluor610 (clone B2D, eBioscience) at 1/100, anti-Helios-PE (clone 22F6, eBioscience) at 1/33, anti-IFN γ -FITC (clone XMG1.2, Biolegend) at 1/500 and anti-IL-4-PE-Dazzle-594 (clone 11B11, Biolegend) at 1/300. Anti-Thy1.1 (clone HIS51, BD Pharmingen) and anti-Thy1.2 (clone 30-H12, eBioscience) at 1/600 were used to discriminate cells in chimeric mice. Additional stainings were performed using anti-c-Myc-PE (clone 9E10, R&D) at 1/20 and rabbit anti-acetyl- α -tubulin (clone D20G3, Cell Signaling) at 1/100 in combination with Zenon Alexa Fluor647 rabbit IgG labeling kit (ThermoFisher Scientific) at 1/200.

Reagents

Colchicine (Sigma) was used at 10 μ M for 30 min at 37°C. Streptavidin (Sigma) was used at 10 μ g/ml. PMA-Iono experiments: Human cells PMA (phorbol 12-myristate 13-acetate) (Sigma) at 100 ng/ml and calcium ionophore A23187 (Sigma) at 500 ng/ml. Mouse cells: Phorbol 12,13-dibutyrate 500 ng/ml and ionomycin at 500 ng/ml (Tocris Bioscience). Brefeldin A (Sigma-Aldrich) at 500 ng/ml. ProLong Gold Antifade (ThermoFisher) mounting medium. DAPI (Life Sciences).

Methods

Cells, siRNA, cell culture and transfection

Jurkat cells were cultured in RPMI-1640 containing 10% fetal calf serum (FCS). Medium was supplemented with 1 mg/ml G418 (Invitrogen) for SLP-YFP expression. Cell lines were mycoplasma free. For siRNA experiments, small double stranded RNA oligonucleotides targeting APC (siAPC) was 5'-GAG AAU ACG UCC ACA CCU U-3' (Dharmacon) and targeting β -globin (siCont) 5'-GGU GAA UGU GGA AGA AGU UTT -5' (Dharmacon). 10⁷ Jurkat

cells were transfected two times at a 24 h interval with 200 pmol of siCont or siAPC with the Neon Transfection system (Life Technologies) at 1400 V, 10 ms, 3 pulses. Cells were harvested and processed for analysis 72 h after the first transfection.

HCT-116 and DLD-1 cells were transfected using Lipofectamine-2000 (Invitrogen) following the manufacturer's instructions.

Peripheral blood of healthy human donors was enriched for isolation of peripheral blood mononuclear cells by Ficoll-Hypaque-Lymphoprep gradient centrifugation for 30 min. Purification of CD4⁺ lymphocytes was performed using the MACS CD4⁺ T Cell Isolation Kit II (Miltenyi Biotec). Cells were cultured overnight in RPMI-1640 medium supplemented with 10% FCS, 1 mM sodium pyruvate and nonessential amino acids. 10⁶ primary CD4⁺ T cells were transfected with 1 nmol of Cont or APC siRNA using Amaxa nucleofection, according to the manufacturer's protocol.

Immunofluorescence, confocal microscopy and image analysis

Coverslips were coated with 10 µg/ml anti-CD3 (MEM92, Interchim), or with poly-L-lysine Poly-L-lysine 0.002% in water, incubating overnight at 4°C. Coverslips were carefully washed with phosphate-buffered saline (PBS) and blocked for 30 min at 37°C with RPMI-1640 medium supplemented with 10% FCS. Cells were dropped on coverslips at 37°C for 3 min or the indicated times, and then fixed with 4% paraformaldehyde for 20 min at room temperature (RT). Shorter fixation time (12 min, 37°C) was used for microtubule detection, followed by methanol incubation for 20 min at -20°C. Cells were washed twice with PBS and incubated for 10 min in PBS supplemented with 5% FCS and 0.05% (vol/vol) saponin (PBS-FCS) to prevent unspecific binding. Primary antibodies were incubated for 1 h at RT. Cells were washed with PBS-FCS three times, incubated with secondary antibodies for 1 h at RT, washed three times with PBS-FCS, once with PBS and coverslips were mounted on microscope slides using 8 µl of ProLongGold Antifade mounting medium with or without DAPI.

Confocal images were acquired with a SP5 confocal microscope (Leica) or LSM 700 confocal microscope (Zeiss) using the Plan-Apochromat 63× objective. Optical confocal sections were acquired with LASX software (Leica) or ZEN software (Zeiss) by intercalating green and red laser excitation to minimize channel cross talk. Confocal optical sections were acquired at 0.17 µm intervals and images were treated by deconvolution with the Huygens Pro Software (version 14.10, Scientific Volume Imaging). A 3D visualization of 3 consecutive confocal sections at the cell-coverslip contact site was produced with Imaris software (Bitplane). Microtubule pattern was analyzed acquiring confocal images at 0.3 µm Z-intervals. Maximum intensity projection of 3 confocal sections at the cell-coverslip contact was generated with ImageJ software. Microtubule pattern quantification was measured by visual observation of two different investigators. Centrosome localization was performed with anti-centrin. Optical sections were acquired at 0.5 µm Z-intervals. Centrin distance from coverslip was quantified with the Acapella software (Perkin Elmer) using a module developed by A. Danckaert (Citech/Imagopole, Institut Pasteur). SLP-76 YFP microclusters were quantified in Jurkat E6.1 cells expressing YFP-SLP-76. Endogenous NFAT microclusters in the presence or absence of colchicine were quantified in Jurkat E6.1 cells. Images were acquired and maximum intensity projections were generated as for microtubule pattern analysis. Automated quantification of microcluster number per area per cell was performed with the Acapella software (Perkin Elmer) using a module previously developed by A. Danckaert (Citech/Imagopole, Institut Pasteur) (Lasserre et al., 2010).

For measurement of NFAT cluster distance to microtubules, confocal images were acquired at 0.2 µm interval and treated by deconvolution with Huygens Pro Software (version 14.10, Scientific Volume Imaging). Deconvoluted images of microtubules and NFAT were segmented into surfaces and spots, respectively, to obtain 3D reconstructions of each cell using the Imaris software (Bitplane) (NFAT segmentation: 0.4 threshold, automatic quality; microtubule segmentation: automatic detection, no smoothing), as advised by J.Y. Tinevez (Citech/Imagopole, Institut Pasteur). Distance of each NFAT (spot) to the closest microtubule (surface) was measured with a custom Spot-to-surface Imaris XT module by Mat-lab (The MathWorks). At least thirty cells were segmented per activation time point. R software was used to generate violin plots and data analysis of the quantified distances.

Live imaging of SLP-YFP microclusters was performed as described before (Lasserre et al., 2011).

Analysis of protein phosphorylation and tubulin acetylation by Western blot

Jurkat T cells were activated with 10 µg/ml soluble anti-CD3 (MEM92, Interchim) and soluble 10 µg/ml anti-CD28 at 37°C for the indicated times, and then incubated with ice-cold PBS supplemented with 2 mM ortho-vanadate and 0.02% sodium azide. Cells were lysed in ice-cold buffer (20 mM Tris pH 7.5, 150 mM NaCl, 0.25% lauryl-β-maltoside, 50 mM NaF, 10 mM Na₄P₂O₇, 1 mM EGTA, 2 mM ortho-vanadate, 1 mM MgCl₂ and protease inhibitor cocktail) for 25 min on ice. Cell lysates were centrifuged at 20800 g for 30 min at 4°C. Equal amount of protein content was loaded in NuPAGE 4-12% Bis-Tris gels (ThermoFisher Scientific) by using the BCA assay Kit (ThermoFisher Scientific). Protein transfer to nitrocellulose blots (LI-COR Biosciences) was performed using the BIO-RAD system. Membranes were saturated with blocking buffer (Rockland) and incubated with primary antibodies for 1 h at RT (anti-phospho-ZAP-70, anti-phospho-PLCγ1, anti-acetylated tubulin and β-tubulin) in blocking buffer. Secondary antibodies-conjugated with Alexa-Fluor680 (Invitrogen) or DyLight800 (Thermo Fisher Scientific) were incubated for 45 min in blocking buffer. Near-infrared fluorescence was imaged and quantified using the Odyssey Li-Cor system (LI-COR Biosciences). Band intensity (arbitrary units) was normalized to control β-tubulin. For a pulled analysis of several experiments, data were normalized as % of siCont at time 0.

For APC detection by Western blot, cells were incubated in lysis buffer (50 mM Tris pH 7.5, 100 mM NaCl, 0.5% NP-40, 5 mM EDTA, 5 mM EGTA, 40 mM β-glycerophosphate, 10 mM NaF, 1 mM ortho-vanadate and protease

inhibitor cocktail) for 5 min at RT. Protein transfer was always performed overnight at 4°C and transfer buffer contained 50 mM Tris, 380 mM Glycine, 7.5% methanol, 0.02% SDS. Membranes were blocked with 5% nonfat dry milk, 1% goat serum, 0.02% Triton X-100 for 2 h at 4°C. Primary Ab (anti-APC, Ali) was incubated overnight at 4°C.

Intracellular calcium concentration analysis

For calcium detection experiments, cells (3×10^6) were loaded with 20 mM fluorescent calcium indicator Fluo-3-AM (Thermo Fisher Scientific) for 30 min in the dark, washed once in RPMI-1640 medium supplemented with 1% FCS and resuspended in 2 ml of the same medium. Intracellular Ca^{2+} concentration was measured before and after activation with 10 μM soluble anti-CD3 (UCHT1) with a 30 s interval for 5 min by flow cytometry with CellQuest software (BD Biosciences) using a FACSCalibur (BD Biosciences). Cells were incubated with 1 mM MnCl_2 or with 2 $\mu\text{g/ml}$ calcium ionophore A23187 (Sigma) to measure, respectively, minimum and maximum Fluo-3-AM signals. FlowJo v9 software (Tree Star) was used for data analysis. Calcium concentration was calculated as described (Kao et al., 1989).

Transcription factor activation analysis by luciferase assays

Transcriptional activity dependent on the transcription factors NFAT and $\text{NF-}\kappa\text{B}$ was measured in Jurkat T, HCT-116 or DLD-1 cells using luciferase-based assays. Cells were co-transfected with 0.1 μg pGL4-Renilla luciferase plasmid (Promega) as a control for transfection efficiency in conjunction with 5 μg NFAT-Firefly luciferase reporter plasmid (Di Bartolo et al., 2007; Roumier et al., 2001), or 5 μg $\text{NF-}\kappa\text{B}$ -Firefly luciferase reporter plasmid (gift of R. Weil Institut Pasteur) (Lasserre et al., 2010), or 5 μg AP1-Firefly luciferase reporter plasmid (Fluhmann et al., 1998). 96 well-plates were coated with 5 $\mu\text{g/ml}$ goat anti-mouse IgG for 3 h at 37°C, washed with PBS, and coated overnight with 25-100 ng/ml anti-CD3 Ab (UCHT1) at 4°C. Coated-plates were washed with PBS and blocked for 1 h with RPMI-1640 medium supplemented with 10% FCS. Cells were activated on plates with addition of 1 $\mu\text{g/ml}$ soluble anti-CD28 Ab for 5 h at 37°C. After stimulation, cells were lysed and processed using the Dual-Luciferase Reporter Assay System (Promega). Luciferase-dependent bioluminescence was measured using an automated dual-injector luminometer (Berthold) with a 2 sec pre-measurement delay and 10 sec post-measurement delay. Firefly luciferase data was normalized with the renilla luciferase data as control of transfection efficiency.

We used the following plasmids to express the different C-terminal APC microtubule binding regions: pCMV-MYC-APC-Cterm (2038–2884 aa) and pCMV-HA-EB1 (2550–2810 aa) and pCMV, as a control of expression vectors encoding no gene (gift of Etienne-Manneville, Institut Pasteur). Jurkat T cells were co-transfected with 7 μg of these plasmids and NFAT-Firefly and pGL4-Renilla luciferase plasmid and were subjected to the same activation described above.

IL2 and NFATC2 mRNA measurements by RT-qPCR

After 72 hours of siRNA transfection, cells were activated with PMA-Iono or with anti-CD3 (100 ng/ml)+CD28, as described in luciferase assays section, for 4h (in Jurkat cells) or 2 hours (in primary CD4^+ T cells).

Total RNA was prepared by using the RNeasy Kit (Qiagen), according to the manufacturer's instructions; on-column DNase I digestion was included to avoid potential DNA contamination. cDNA was generated from 100 ng (CD4^+ lymphocytes from healthy donors) or 500 ng (Jurkat cells) of total RNA using iScript cDNA synthesis kit (BIO-RAD). In all cases, 2 ml of a 2.5 dilution of generated cDNA solution was used as a template for real-time PCR (qPCR). Gene products were quantified by qPCR with the ABI PRISM 7900HT sequence detection system, using FastStart Universal SYBR Green PCR master mix (Roche). Each experiment was performed at least in triplicate and qPCR quantifications were performed in triplicates. qPCR quantity values were calculated by the Relative Standard Curve Method. Values were normalized to the mRNA expression of the beta-2-microglobulin (B2M) or TATA Box Binding Protein (TBP) housekeeping genes in Jurkat cells; or to succinate dehydrogenase complex, flavoprotein subunit A (SDHA) or TBP in CD4^+ lymphocytes. Primer sequences were as follows:

IL2-F: 5'-ACCTCAACTCCTGCCACAAT-3'/ R: 5'-TGAGCATCCTGGTGAGTTTG-3'
NFATC1-F: 5'-AGGAAGTACAGCCTCAACGG -3'/ R: 5'- CTGGTGTACTGGGTGGTGT -3'
NFATC2-F: 5'- AAATCGGCTCCAGAATCCA -3'/ R: 5'-GATGCTGCAGATGGGAATGG-3'
B2M-F: 5'- TGACTTTGTCACAGCCCAAGATA-3'/ R: 5'-AATGCGGCATCTTCAAACCT-3'
SDHA-F: 5'-TGGAACAAGAGGGCATCTG-3'/ R: 5'-CACCAGTGCATCAAATTCATG-3'
TBP-F: 5'-CACGAACCACGGCACTGATT-3'/ R: 5'-TTTTCTTGCTGCTGCCAGTCTGGAC-3'

Nuclear NFAT detection by cytoplasm/nucleus cell fractionation and immunofluorescence.

Nuclear NFAT was quantified by western blot analysis of cells fractionated for nucleus and cytoplasm separation. Cells were activated with 10 $\mu\text{g/ml}$ soluble anti-CD3 and 10 $\mu\text{g/ml}$ anti-CD28 Abs for the indicated times at 37°C, and ice-cold PBS supplemented with 2 mM ortho-vanadate and 0.02% sodium azide was added to stop cell stimulation. Cells were incubated in ice-cold low-salt lysis buffer (10 mM KCl, 10 mM HEPES, 0.1 mM EDTA, 0.1 mM EGTA, 1 mM DTT, 50 mM NaF, 10 mM NaPP and protease inhibitor cocktail) for 15 min on ice. Detergent Nonidet P-40 (Sigma) was added (0.45% v/v final) to break the cytoplasmic membranes without altering the nuclear membranes. Cell lysates were vortexed for 10 s and immediately centrifuged at 20800 g for 30 min at 4°C. Supernatants were recovered in pre-cooled tubes and kept as cytosolic fractions. Cell pellets containing cell nuclei were further solubilized in ice-cold high-salt buffer (20 mM Tris-HCl pH 8.0, 1% SDS, 2 mM EDTA and protease inhibitor cocktail). Nuclear proteins including the chromatin fraction were solubilized by sonication (10 sec 3 times at 60% power) and centrifuged 12000 g for 15 min. Supernatants were recovered as nuclear fractions. Protein content was measured using the BCA assay Kit

(ThermoFisher Scientific). Western blot was performed using anti-NFAT1 (NFATC2) (Cell Signaling), anti-ZAP70 (Becton Dickinson) and histone-3 (Abcam) of nuclear or cytoplasmic lysates. NFAT band intensity (arbitrary units) was normalized to ZAP-70 cytoplasmic control or histone-3 (H3) nuclear control. For a pulled analysis of several experiments, data were normalized as % of siCont at time 0.

Nuclear NFAT was measured immunofluorescence in the Dapi mask using ImageJ (free software) in cells forming conjugates with antigen-presenting cells (Raji), prepared as described before (Roumier et al., 2001).

Mixed bone marrow chimeras

Mixed bone marrow chimeras were generated using standard procedures. *Thy1a* (Thy1.1, WT for Apc) recipient mice were lethally irradiated with 1100 rads, then injected intravenously via the retro-orbital sinus with 2×10^7 cell comprised of a 50:50 mixture of bone marrow cells from Thy1.2 Apc^{Min/+} and Thy1.1 WT mice. Chimeras were sacrificed for analysis 9 weeks after engraftment.

Intestinal leukocyte isolation

Intestinal leukocyte isolation procedure was adapted from Lefrançois and Lycke (Lefrancois and Lycke, 2001). Briefly, the jejunum of the small intestine was removed, flushed extensively with PBS, opened longitudinally, chopped crudely, and then incubated in PBS supplemented 5% FCS, 2 mM EDTA, and 1 mM dithioerythritol for 20 min incubations at 37°C to remove the epithelial cell layer. The remaining tissue was digested with 300 U/ml collagenase IV (Worthington Biochemical), 50 U/ml hyaluronidase (Worthington Biochemical), and 5 mg/ml DNase I (Appllichem) for 30 min at 37°C, then dispersed through a 70 mm filter to release lamina propria cells. Leukocytes were separated over discontinuous 40% 70% Percoll (GE Healthcare) density gradients with centrifugation at 500 g for 20 min.

Intracellular cytokine staining

Lymphocytes isolated from lamina propria were stimulated for 4 h with 500 ng/ml ionomycin (Tocris Bioscience), 500 ng/ml phorbol 12,13-dibutyrate (Tocris Bioscience), and 1 mg/ml brefeldin A (Sigma-Aldrich). Cells were stained to detect CD4, TCR β and CD45, and low affinity Fc receptor interactions were blocked with anti-Fc γ R2/3 (clone 93) (Biolegend). Dead cells were routinely excluded from analyses on the basis of staining with fixable viability dye eFluor780 (Affymetrix eBioscience). Robust coordinate staining for Foxp3 and cytokines was achieved using the BD CytoFix CytoPerm kit (BD Biosciences) and staining overnight for intracellular proteins using reduced concentrations of antibodies (Burton et al., 2014). Analyses were restricted to single cells using FSC-H/W signals. Data were acquired using DIVA software on an LSRFortessa cytometer (BD Biosciences) with 405 nm, 488 nm, 561 nm and 640 nm lasers, and analyzed using FlowJo v9 (Tree Star).

NFAT nuclear localization in intestinal Tregs by ImageStream Flow Cytometry

CD4⁺ lymphocytes were purified from intestinal lamina propria leukocyte cell suspensions by negative selection using MACS magnetic beads and a cocktail of antibodies directed against CD8a (53-6.7, BD Pharmingen), CD11b (M1/70, BD Pharmingen), CD11c (HL3, BD Pharmingen), CD19 (MB19-1, eBioscience), B220 (RA3-6B2, BD Pharmingen), Fc ϵ R1a (MAR-1, eBioscience), Siglec F (E50-2440, BD Pharmingen), Gr-1 (RB6-8C5, BD Pharmingen) and c-Kit (2B8, eBioscience). CD4⁺ lymphocytes were incubated with anti-CD4-PerCP-Cy5.5 (RM4-5, Biolegend), anti-TCR β -FITC (H57-597, Biolegend), anti-Fc γ R2/3 (clone 93, Biolegend) and fixable viability dye eFluor780 (eBioscience). Cells were fixed, permeabilized and stained overnight using the BD CytoFix CytoPerm kit (BD Biosciences) as described for intracellular cytokine assays. Anti-Foxp3-PE (FJK-16s, eBioscience) and anti-NFAT1 (Cell Signaling) Ab at 1/100 was used in addition with 500 ng/ml DAPI (Invitrogen) and Zenon anti-rabbit IgG labeling reagent AF647 (ThermoFisher Scientific) at 1/200. Cells were analyzed using the ImageStreamX[®] Mark II Imaging Flow Cytometer (Millipore).

At least 1000 CD4⁺TCR β ⁺Foxp3⁺ cells were scored using the nuclear localization module of the INSPIRE and IDEAS software (Millipore). Nuclear NFAT was quantified as similarity (similarity dilate) of the NFAT and DAPI masks of the images.

Supplemental References

- Burton, O.T., Noval Rivas, M., Zhou, J.S., Logsdon, S.L., Darling, A.R., Koleoglou, K.J., Roers, A., Houshyar, H., Crackower, M.A., Chatila, T.A., and Oettgen, H.C. (2014). Immunoglobulin E signal inhibition during allergen ingestion leads to reversal of established food allergy and induction of regulatory T cells. *Immunity* *41*, 141-151.
- Di Bartolo, V.B., Montagne, B., Salek, M., Jungwirth, B., Carrette, F., Fournane, J., Sol-Foulon, N., Michel, F., Schwartz, O., Lehmann, W.D., and Acuto, O. (2007). A novel pathway down-modulating T cell activation involves HPK-1-dependent recruitment of 14-3-3 proteins on SLP-76. *J Exp Med* *204*, 681-691.
- Fluhmann, B., Zimmermann, U., Muff, R., Bilbe, G., Fischer, J.A., and Born, W. (1998). Parathyroid hormone responses of cyclic AMP-, serum- and phorbol ester-responsive reporter genes in osteoblast-like UMR-106 cells. *Mol Cell Endocrinol* *139*, 89-98.
- Kao, J.P., Harootyan, A.T., and Tsien, R.Y. (1989). Photochemically generated cytosolic calcium pulses and their detection by fluo-3. *J Biol Chem* *264*, 8179-8184.

- Lasserre, R., Charrin, S., Cuche, C., Danckaert, A., Thoulouze, M.I., de Chaumont, F., Duong, T., Perrault, N., Varin-Blank, N., Olivo-Marin, J.C., *et al.* (2010). Ezrin tunes T-cell activation by controlling Dlg1 and microtubule positioning at the immunological synapse. *Embo J* *29* 2301-2314.
- Lasserre, R., Cuche, C., Blecher-Gonen, R., Libman, E., Biquand, E., Danckaert, A., Yablonski, D., Alcover, A., and Di Bartolo, V. (2011). Release of serine/threonine-phosphorylated adaptors from signaling microclusters down-regulates T cell activation. *J Cell Biol* *195*, 839-853.
- Lefrancois, L., and Lycke, N. (2001). Isolation of mouse small intestinal intraepithelial lymphocytes, Peyer's patch, and lamina propria cells. *Curr Protoc Immunol Chapter 3*, Unit 3 19.
- Roumier, A., Olivo-Marin, J.C., Arpin, M., Michel, F., Martin, M., Mangeat, P., Acuto, O., Dautry-Varsat, A., and Alcover, A. (2001). The membrane-microfilament linker ezrin is involved in the formation of the immunological synapse and in T cell activation. *Immunity* *15*, 715-728.